Non-canonical immunomodulatory activity of complement regulator C4BP limits the development of lupus nephritis

Journal:	*Kidney International*
Manuscript ID	KI-12-18-1865.R2
Article Type:	Basic Research
Date Submitted by the Author:	n/a
Complete List of Authors:	Luque, Ana; IDIBELL Serrano, Inmaculada; IDIBELL Ripoll, Elia ; IDIBELL Malta, Catarina; IDIBELL Goma, Montse; Hospital Universitari de Bellvitge Blom, Anna; Lund University Grinyó, Joseph; Hospital Universitari de Bellvitge Rodríguez de Córdoba, Santiago; Centro de Investigaciones Biologicas Torras, Juan; Hospital Universitari de Bellvitge Aran, Josep; IDIBELL
Subject Area:	Chronic Kidney Injury, Immunology, Renal Pathology
Keywords:	complement, gene expression, glomerulonephritis, inflammation, macrophages, systemic lupus erythematosus

SCHOLARONE™
Manuscripts

Non-canonical immunomodulatory activity of complement regulator C4BP limits the development of lupus nephritis

Ana Luque[1,6], Inmaculada Serrano[1,6], Elia Ripoll[2], Catarina Malta[1], Montserrat Gomà[3], Anna M. Blom[4], Josep M. Grinyó[2], Santiago Rodríguez de Córdoba[5], Joan Torras[2] and Josep M. Aran[1]

[1] Immune-inflammatory Processes and Gene Therapeutics Group, IDIBELL, 08908 L'Hospitalet de Llobregat, Barcelona, SPAIN.

[2] Nephrology Department, Bellvitge University Hospital, Experimental Nephrology Lab., University of Barcelona and IDIBELL, 08908 L'Hospitalet de Llobregat, Barcelona, SPAIN.

[3] Pathology Department, Bellvitge University Hospital, IDIBELL, 08908 L'Hospitalet de Llobregat, Barcelona, SPAIN.

[4] Lund University, Department of Translational Medicine, Section of Medical Protein Chemistry, 21428 Malmö, SWEDEN.

[5] Centro de Investigaciones Biológicas (CSIC) and Ciber de Enfermedades Raras (CIBERER), 28040 Madrid, SPAIN.

[6] Equal contributors

Correspondence should be addressed to J.M.A. (jaran@idibell.cat):

Dr. Josep M. Aran
Human Molecular Genetics Group
Institut d'Investigació Biomèdica de Bellvitge (IDIBELL)
Hospital Duran i Reynals
Gran Vía s/n km 2,7
08908 L'Hospitalet de Llobregat
Barcelona, SPAIN
Phone: +34 (93) 2607428
Fax: +34 (93) 2607414
E-mail: jaran@idibell.cat

Running title: C4BP(β-) reduces lupus nephritis
Keywords: C4BP(β-), lupus nephritis, dendritic cells, inflammation, immunomodulation, ectopic lymphoid structures

For Peer Review Only

ABSTRACT

Lupus nephritis (LN) is a chronic autoimmune-inflammatory condition that can lead to end-stage renal disease because of the breakage of immune self-tolerance occurring in systemic lupus erythematosus (SLE) patients. Presently available immunosuppressive treatments for LN are suboptimal and can induce significant side effects. We have recently characterized a novel immunomodulatory activity on the minor isoform of the classical pathway complement inhibitor, C4BP(β-). We show here that C4BP(β-) treatment prevented the development of proteinuria and albuminuria, decreased significantly the formation of anti-dsDNA antibodies and, locally, mitigated renal glomerular IgG and C3 deposition and generation of apoptotic cells, with the consequent histological improvement and increased survival in lupus-prone mice. The therapeutic efficacy of C4BP(β-) was analogous to that of the broad-acting immunosuppressant cyclophosphamide (CYP). Remarkably, a comparative transcriptional profiling analysis revealed that: 1) the renal gene expression signature resulting from C4BP(β-) treatment turned out to be 10 times smaller than that induced by CYP treatment, and 2) C4BP(β-) immunomodulation induced significant downregulation of LN relevant transcripts indicating immunopathogenic cell infiltration, including activated T cells (*Lat*), B cells (*Cd19, Ms4a1, Tnfrsf13c*), inflammatory phagocytes (*Irf7*) and neutrophils (*Prtn3, S100a8, S100a9*). Furthermore, cytokine profiling and immunohistochemistry confirmed that C4BP(β-), through systemic and local CXCL13 downregulation, was able to prevent ectopic lymphoid structures neogenesis in aged LN mice. Thus, because of its anti-inflammatory and immunomodulatory activities and high specificity, C4BP(β-) could be considered for further clinical development in SLE patients.

For Peer Review Only

TRANSLATIONAL STATEMENT

Lupus nephritis (LN) is a chronic autoimmune-inflammatory condition for which current treatments with NSAIDs and immunosuppressive drugs, and even with new biologics, remain unsatisfactory and/or induce non-specific adverse events. Therefore, novel therapeutic agents are needed, with increased potency, selectivity and safety profiles. We have recently characterized a novel immunomodulatory activity in the minor isoform of the complement inhibitor C4BP(β-). Here we show that this non-canonical activity limits the evolution of LN in lupus-prone mice, preventing the development of CXCL13-driven renal ectopic lymphoid structures. Thus, the anti-inflammatory and tolerogenic functions of C4BP(β-) might contribute significantly to restore immune homeostasis and to achieve better outcomes in LN management.

For Peer Review Only

INTRODUCTION

Systemic lupus erythematosus (SLE) is heterogeneous in nature regarding organ involvement, clinical manifestations and severity, although the most life-threatening trait is progressive nephritis, leading to end-stage renal disease.[1] A key early event in lupus nephritis (LN) involves impaired myeloid phagocytes which, unable to clear apoptotic cell debris and/or neutrophil extracellular traps (NETs), initiate a TLR-mediated pro-inflammatory program leading to direct activation of effector T cells and indirect activation of B cells through the production of important mediators such as B-cell activating factor (BAFF).[2–4] In turn, stimulation and increased survival of B cells leads to the production of pathogenic autoantibodies against nuclear components (e.g., nucleic acids and histones), local parenchymal immune complex (IC) deposition and activation of the complement system, and additional production of pro-inflammatory chemokines and cytokines such as IFN-I.[5] These events induce a self-sustaining feed-forward loop of chronic inflammation and progressive glomerular, tubulointerstitial and endothelial kidney damage. In fact, focal infiltration and progressive organized aggregation of immune cells is the hallmark of autoreactive ectopic lymphoid structures (ELS), also known as tertiary lymphoid organs, developing in both human and murine LN.[3,6] Thus, circulating and resident immune cells become important causative agents in the promotion of pro-inflammatory renal injury through ELS expansion, which maximizes the encounters between autoantigens, antigen-presenting cells and lymphocytes, important for the local initiation and maintenance of adaptive immune responses. This knowledge framework offers insight for the development of targeted immunotherapy interventions able to halt tissue damage and chronic inflammation by restoring operational immune tolerance. Accordingly, a new group of biologics, mostly neutralizing antibodies directed against pro-inflammatory molecular targets or cellular leukocyte subsets, such as rituximab, eculizumab, or belimumab, are on pre-clinical or early clinical development aiming to become efficient immunomodulatory agents without the unwanted effects

For Peer Review Only

of broad-based immunosuppression displayed by conventional therapy, such as long-term toxicity by cyclophosphamide (CYP) and steroids. However, thus far the therapeutic benefit of biologics for inflammatory renal disease has been limited.[7]

Synthesized mainly in the liver, C4b-binding protein (C4BP), a main regulator of the complement system, is relatively abundant in the circulation as a major heterooligomer (α7β1, or C4BP(β+)), and a minor homooligomer (α7β0, or C4BP(β-)) that becomes significantly upregulated under inflammatory conditions (e.g., acute phase response).[8,9] Both isoforms are able to inhibit the classical and the lectin pathways of complement activation.[10] In addition C4BP(β+), through its β-chain, forms a high-affinity complex with protein S (PS), which endows it with additional roles in coagulation and in apoptotic cell binding.[11,12] Alternatively, we have recently described a novel anti-inflammatory and immunomodulatory activity of human C4BP(β-) capable to induce a myeloid-derived suppressor cell (MDSC)-like phenotype through its direct action on monocyte-derived dendritic cells (Mo-DCs), an established model of inflammatory DCs.[13]

In this study we aimed to assess the therapeutic potential of C4BP(β-) in experimental autoimmune LN. We show that C4BP(β-), but not C4BP(β+), mitigates the development of renal pathology in lupus-prone NZBW F1 and MRL-*lpr* mice, preventing the neogenesis of autoreactive ELS, which hold a key role locally enhancing renal maladaptive immune response and chronic inflammation.

For Peer Review Only

RESULTS

C4BP(β-) preserves renal function in lupus-prone NZBW F1 mice

As we previously reported,[13] human C4BP(β-) confers a semi-mature, anti-inflammatory phenotype to LPS-matured Mo-DCs from healthy individuals. Thus, we first sought to confirm the immunomodulatory activity of human C4BP(β-) in a mouse background. C4BP(β-) treatment prevented the upregulation of CD80 and CD86 co-stimulatory molecule expression by cultured bone marrow-derived DCs stimulated with the TLR7 agonist gardiquimod, of relevance in LN pathology.[14] (**Supplementary Figure S1**).

To assess the therapeutic potential of C4BP(β-) in experimental autoimmune LN we designed an intraperitoneal administration schedule for this human plasma-purified protein into lupus-prone NZBW F1 mice (**Figure 1a**). Proteinuria is the most prominent and life-threatening sign in LN mice. It reflects renal dysfunction and closely correlates with disease outcome. In PBS vehicle-treated control mice, proteinuria started to develop at week 28 and progressed exponentially to severe proteinuria (> 300 mg/kg) by week 34 (8.5 months of age) up to the end of the study (week 36). In comparison, the onset of proteinuria was delayed until the end of the study by C4BP(β-) treatment, and was significantly reduced from that of the control PBS vehicle-treated group (p<0.0001) (**Figure 1b**). Thus, neither the standard CYP treatment group nor the C4BP(β-) treatment group did develop noteworthy proteinuria over time. Nonetheless, a slight upturn in proteinuria, particularly evident as microalbuminuria, appeared by week 36 in the C4BP(β-) treatment group, compared with the CYP treatment group (**Figure 1c**). This apparently decreased therapeutic efficacy of C4BP(β-) at later stages of treatment could reflect accelerated clearance due to the development of an immune xenoresponse against the administered human protein in the NZBW F1 immunocompetent mice.[15] Certainly, repeated

For Peer Review Only

C4BP(β-) administration induced the production of anti-C4BP(β-)-specific antibodies that were detected in the sera of the treated animals, peaking around week 32 (**Supplementary Figure S2**).

In an additional set of experiments, we confirmed that as little as 50 μg/mouse of purified C4BP(β-) produced in HEK293 mammalian cells, administered biweekly and subcutaneously, was still able to ameliorate the renal function and increase the survival of nephritic NZBW F1 mice, despite the comparable immunogenicity of both plasma-purified and recombinant C4BP(β-) (**Supplementary Figure S3**).

C4BP(β-) attenuates the development of anti-dsDNA antibodies and ameliorates histologic damage in the kidneys of lupus-prone NZBW F1 mice

The autoantibody titers directly reflect autoimmunity status. In the vehicle PBS-instilled control NZBW F1 mice, the serum anti-dsDNA total Igs began to progressively increase at 5-6 months of age (week 20-24). Within another 3 months the anti-dsDNA Igs reached its highest titer, which persisted thereafter (**Figure 2a**). In comparison, mice from the C4BP(β-) group had a sustained lower level of autoantibodies throughout the analysis period (weeks 28 to 36) ($p<0.05$). As expected, the standard CYP treatment group also showed reduced anti-dsDNA autoantibody levels.

Even though proteinuria reflects the severity of renal dysfunction, the pathological study directly reveals tissue damage in LN. Common characteristics of severe nephritis in lupus kidneys include proliferative changes in the mesangial and endothelial cells of the glomeruli, capillary basement membrane thickening, severe interstitial infiltrates, tubular atrophy and large protein casts. **Figure 2b-d** compares representative renal histologic findings in the C4BP(β-) and CYP treatment groups and in the PBS vehicle control group. The 9-month old control PBS mice exhibited typical nephritis changes, including significantly enlarged and hypercellular glomeruli

For Peer Review Only

(**Figure 2c**), interstitial inflammation and widespread proteinaceous tubular casts, as expected from their severe proteinuria. Conversely, age-matched mice in both the C4BP(β-) and CYP treatment groups presented almost intact glomeruli, tubules and interstitium, with lower pathologic scores (**Figure 2b-d**). Thus, C4BP(β-) treatment attenuated the development of anti-dsDNA antibodies, protecting kidneys from autoantibody induced damage.

Renal IC deposits and apoptotic cells are significantly reduced in C4BP(β-)-treated lupus-prone NZBW F1 mice

IC deposits in the kidneys provide direct evidence for the pathogenicity of the autoantibodies in the target organ and are associated with nephritis in NZBW F1 mice.[16] We stained renal cryosections for IgG and C3, two major components in IC. In the vehicle-treated PBS control mice, there was pronounced IgG and C3 deposition in the glomeruli (**Figure 3a**) which was markedly diminished both in C4BP(β-)-treated and in CYP-treated mice ($p<0.0001$). Therefore, the IC deposits were consistent with the renal histopathological changes.

Impaired clearance of apoptotic debris and IgG ICs by phagocytes is considered to be one of the main causes of inflammation associated with LN.[17] Indeed, TUNEL analysis revealed widespread presence of both intraglomerular and extraglomerular apoptotic cells in the kidneys of PBS-treated mice. In contrast, both C4BP(β-)- and CYP-treated mice had essentially no apoptotic cells in the renal cortex (**Figure 3b**), correlating with reduced kidney damage.

C4BP(β-) targets molecular/cellular hallmarks of LN

For Peer Review Only

To gain further insight into the local immunomodulatory events induced by C4BP(β-) treatment at the molecular and cellular level, we performed a comparative transcriptional profiling of renal tissue from C4BP(β-)-treated, CYP-treated, and PBS-treated control NZBW F1 mice. The in-house designed array included 377 genes involved in SLE pathology (**Supplementary Table S1**). Remarkably, an initial evaluation of the expression profiles of C4BP(β-)-treated and CYP-treated mice, both relative to PBS-treated control mice, unveiled a drastically different appearance in their overall shape (**Figure 4a**). Accordingly, only 24 differentially expressed transcripts (FC ≥ 1.8) were apparent between the C4BP(β-)-treated and the PBS-treated kidneys (**Supplementary Table S2**). Conversely, the same analysis when comparing CYP-treated and PBS-treated kidneys yielded 224 differentially regulated transcripts (**Supplementary Table S3**). Taking into account the comparable therapeutic efficacies of C4BP(β-) and CYP treatments in LN mice, as perceived from the previously analyzed parameters, this outcome suggests more specific immunomodulation induced by C4BP(β-) over the immunosuppressant CYP in LN NZBW F1 mice.

An additional gene-interaction based bioinformatics analysis of the analyzed genes revealed that relevant biological functions modulated by C4BP(β-)-treatment involved reduced renal leukocyte migration, particularly of myeloid cells, and consequently, a decreased quantity and activation of infiltrated mononuclear leukocytes, predominantly B lymphocytes (**Supplementary Table S4**). Conversely, a great number of additional relevant pathways, such as the complement pathway, were appreciably regulated only by CYP treatment (data not shown) suggesting increased toxicity of the immunosuppressant CYP over C4BP(β-).

Next, we validated the above results obtained with the microfluidics cards by analyzing renal tissue from individual mice within each group by RT-qPCR, and interrogating the transcripts that showed differential regulation by C4BP(β-) at FC ≥ 2.0 in the array. We confirmed significant differential C4BP(β-)-mediated downregulation of 8 transcripts: *Irf7, Lat,*

For Peer Review Only

Cd19, Ms4a1 (Cd20), Tnfrsf13c (BAFFR), Prtn3, S100a8 and S100a9 (**Figure 4b**). All but *S100a8 and S100a9*, encoding the S100a8/S100a9 complex calprotectin involved in inflammasome activation and myelopoiesis induction, were found also significantly downregulated by CYP treatment. Strikingly, while Irf7 is a key transcription factor involved in the type I IFN pathway activated by innate sensors, such as TLR7/8, as a consequence of impaired lysosomal maturation of SLE phagocytes,[2] all other transcripts are cellular markers specific for activated T lymphocytes (*Lat*), B lymphocytes (*Cd19, Ms4a1, Tnfrsf13c*), and neutrophils (*Prtn3, S100a8, S100a9*). This again indicates significant leukocyte infiltration, suggesting a lack of immune tolerance as the underlying cause of LN pathology in the kidneys of PBS-treated control NZBW F1 mice which, however, could be mitigated by both C4BP(β-) and standard CYP treatment. Further, assessment of network crosstalk between the C4BP(β-) gene set including the above 8 significantly regulated genes and the KEGG pathways using PathwAX reflected significant (FDR ≤ 0.05) depletion of immune hematopoietic cells and, particularly, of the B cell signaling and the pro-inflammatory NF-κB pathways in C4BP(β-)-treated renal tissue compared with the PBS-treated, nephritic tissue (**Table 1**).

C4BP(β-) modulates the cytokine signature of lupus-prone NZBW F1 mice

To complement the transcriptional profiling results obtained, we examined the presence of inflammatory cytokines in the sera of the treated NZBW F1 mice at the end of the study. Remarkably, a cytokine array including 40 mouse cytokines, chemokines and acute phase proteins evidenced CXCL13 as the unique cytokine differentially abundant, present in PBS-treated mice but absent in C4BP(β-)-treated or CYP-treated mice (**Figure 5a**). This homeostatic B cell-attracting chemokine, produced by macrophages and dendritic cells, is extremely relevant

For Peer Review Only

in SLE renal pathology. We confirmed the array findings assessing the CXCL13 levels in the sera of individual mice through a specific ELISA assay (**Figure 5b**).

An identical cytokine analysis, using renal tissue extracts instead of sera, endorsed differential expression of CXCL13 and, additionally, revealed local presence of the C5/C5a complement components, and of the IL1 family members IL1 receptor antagonist (IL1ra; IL-1F3) and IL1β (**Figure 5c and 5d**). Thus, local increase of these inflammatory factors, while apparent in PBS-treated kidneys, could be prevented by C4BP(β-) or CYP treatment.

C4BP(β-) treatment prevents leukocyte infiltration and the development of ELS in the renal parenchyma of lupus-prone NZBW F1 mice

LN, a chronic inflammatory condition, features significant leukocyte infiltration over time, as suggested by our transcriptional profiling data. Indeed, a thorough immunohistochemical examination regarding the presence of inflammatory leukocyte markers in the renal cortex of 36 weeks old PBS-treated NZBW F1 mice evidenced positive staining, mainly perivascular and, occasionally, periglomerular, not only for activated T cells (Lat) and B cells (CD19), but also for different myeloid cell populations: neutrophils (Gr1), interstitial monocytes/macrophages (F4/80), and dendritic cells (CD11c). In contrast, the above markers were barely present (F4/80) or virtually absent in both C4BP(β-)-treated or CYP-treated mice (**Figure 6**).

The chemokine CXCL13 holds a key role recruiting and organizing nodular aggregates of B cells, activated T cells and DCs surrounded by neo-lymphatic vessels termed ELS.[18] Indeed, we confirmed the presence of multiple ELS in the cortex of PBS-treated NZBW F1 nephritic mice by hematoxilin and eosin staining and by T cell (Lat) and B cell (Cd19) immunostaining (**Figure 7**). In contrast, C4BP(β-) immunomodulatory activity prevented the development of

For Peer Review Only

local inflammatory ELS in these mice, which correlated with reduced autoantibody anti-dsDNA formation and renal function improvement.

The complement inhibitory activity of C4BP does not affect LN pathology in lupus-prone NZBW F1 mice

To assess whether C4BP-mediated complement inhibition could be responsible for the improvement of LN we performed a comparative study administering equal amounts of either the minor C4BP(β-) isoform, sustaining both complement inhibitory and immunomodulatory activities, or the major isoform C4BP(β+), holding only the complement inhibitory but not the immunomodulatory activity,[13] into NZBW F1 mice. C4BP(β-)-treated mice showed reduced proteinuria, decreased anti ds-DNA and blood urea nitrogen (BUN) levels, improved renal histology with minimal immune cell infiltration and a higher survival rate when compared with C4BP(β+)-treated mice (**Supplementary Figure S4**). Furthermore, we analyzed the activity of the classical pathway of complement in fresh serum extracted from NZBW F1 mice previously (week 21), and at several points during C4BP treatment (weeks 25, 29 and 33). The complement activity was nearly within the normal range in young mice, before starting C4BP treatment, but was concomitantly reduced with the progression of LN pathology in both the PBS- and C4BP(β+)-treated mice (**Supplementary Figure S5)**. A severe drop in hemolytic complement in advance of clinical renal disease has been reported in these mice, which suggested consumption by ICs.[19] In contrast, C4BP(β-) treatment significantly precluded hypocomplementemia at the early stages of treatment. Nevertheless, complement exhaustion could not be prevented at the later stages of treatment, possibly due to lack of C4BP(β-) immunomodulatory efficacy because of the development of the anti-human C4BP(β-) immune xenoresponse, as previously indicated.

For Peer Review Only

Therapeutic efficacy of C4BP(β-) in lupus-prone MRL-*lpr* mice

We substantiated the above results and the overall therapeutic efficacy of C4BP(β-) immunomodulation using MRL-*lpr* mice as an alternative spontaneous LN model. Thus, a weekly treatment schedule using 100 μg C4BP(β-)/mouse starting at 10 weeks of age not only mitigated the development of proteinuria, increased survival, preserved renal histology preventing ectopic lymphoid tissue formation and increased the survival rate, but also ameliorated dermatitis and vasculitis, other SLE pathological traits developing in the MRL-*lpr* model (**Figure 8**).

For Peer Review Only

DISCUSSION

In this report we demonstrate the benefit of human C4BP(β-), an acute phase protein with a well-known complement inhibitory function and with a previously unrecognized and recently characterized anti-inflammatory and tolerogenic activity towards inflammatory DCs, in two spontaneous models of autoimmune LN: NZBW F1 and MRL-*lpr* mice. A prior study has reported the potential of human C4BP(β-) inhibiting the development of autoimmune arthritis in mice, which was exclusively attributed to its complement inhibitory activity.[20] However, the fast systemic clearance of human C4BP(β-) when administered to mice [20] suggests that an alternative mode of action of C4BP(β-) might contribute significantly to the substantial therapeutic effect noticed in the arthritis models employed. In fact, we show here that the major C4BP(β+) isoform, holding the same complement inhibitory activity than C4BP(β-) but lacking immunomodulatory activity, [13] does not affect the development of LN from NZBW F1 mice. Furthermore, C4BP(β-), but not C4BP(β+), was able to prevent in these mice the progress to hypocomplementemia, an important marker for the presence of IC-mediated disease. It has been shown that complement titers fall significantly with renal disease progression, concomitantly with the appearance of anti-DNA autoantibodies in serum and of C3 Igs in renal glomeruli.[19] Nonetheless, we acknowledge C4BP(β-) action limiting both C3 deposition in the glomeruli and the presence of C5/C5a in the renal cortex of C4BP(β-)-treated NZBW F1 mice. In fact, inhibition of complement activity at different points, such as through mAb-mediated C5 blockade,[21] using C3a[22] or C5a[23] receptor antagonists, or by CR2-targeted complement inhibitors: CR2-DAF,[24] CR2-Crry,[25] or CR2-FH[26] has proven useful in the amelioration of LN. Yet the deposition of ICs or complement does not seem sufficient for renal pathology.[27–29] In our study, while CYP, a broad-acting immunosuppressant and standard of care treatment for the most severe manifestations of SLE,[30] induced transcriptional downregulation of several

For Peer Review Only

complement effectors in renal tissue from NZBW F1 mice, no such modulation was observed upon C4BP(β-) treatment. Nevertheless, the therapeutic efficiency of C4BP(β-) was comparable to that exhibited by CYP. Moreover, scaling down 10-fold the subcutaneous dosage of C4BP(β-) to 50 μg/mouse and setting up a bi-weekly administration schedule, was still able to significantly ameliorate disease severity in LN mice.

Mouse C4BP lacks both the β-chain,[31] and two complement control protein domains (CCPs) in the α-chain homologous to CCP5 and CCP6 from the human C4BP α-chain.[32] We have previously described that CCP6 is necessary for the immunomodulatory activity of human C4BP(β-).[13] Hence, the mouse constitutes a suitable animal model to assess the immunomodulatory activity of human C4BP(β-) without interference from endogenous mouse C4BP. Certainly, C4BP knock-out did not develop any autoimmune phenotype, and did not modify disease severity in MRL-*lpr* LN mice,[33] stressing the relevance of human C4BP(β-) immunomodulation in NZBW F1 LN pathology.

Both C4BP(β-),[13] and the major alternative pathway complement inhibitor FH,[34] through as yet unknown receptor(s), directly counteract cellular immune-inflammatory activation by inducing an anti-inflammatory and tolerogenic state on monocyte-derived DCs analogous to that recently described for monocytic MDSCs, which confer suppressive activity toward multiple myeloid and lymphoid cell subsets.[35,36] Remarkably, myeloid cells seem to take a central pathogenic role in SLE owing to inefficient clearance of apoptotic cell debris and autoantigen-autoantibody ICs by phagocytes because of defects in lysosomal maturation.[2] Thus, FcγRI-mediated activation of DC and macrophage innate sensors, through accumulated IgG-ICs in their surfaces, seems to occur prior to significant B cell expansion, IFN-α and BAFF secretion, and LN progression.[17] For example, RNA sensing by conventional DCs through TLR7 has been reported to be critical to the development of LN.[37] C4BP(β-) is able to prevent TLR4- and TLR7-mediated activation of monocyte-derived DCs ([13], and data not shown). Accordingly,

For Peer Review Only

immunomodulatory C4BP(β-) administration in our NZBW F1 LN model seemed to preclude glomerular and interstitial apoptotic cell accumulation and/or apoptotic debris coating of myeloid cells, either preventing cell dying or increasing their renal clearance.

Strikingly, at the molecular level, a comparative analysis of the transcriptional fingerprints of C4BP(β-), CYP, and the vehicle PBS induced in renal tissue from 36-week old NZBW F1 mice uncovered the high specificity of C4BP(β-) treatment respect to the standard CYP regimen. Thus, setting the threshold FC to ± 1.8, only 24 transcripts (6.4 % of the SLE genes arrayed) were regulated by C4BP(β-) compared with 224 transcripts (59.4 % of the SLE genes arrayed) by CYP, nevertheless both conferring analogous functional improvements in the LN NZBW F1 kidneys. This points out to increased safety due to a much more focused and specific action of C4BP(β-)-mediated immunomodulation as compared with the known toxicity profile concomitant to CYP global immunosuppression.

The resulting C4BP(β-) transcriptional profile also revealed exclusive downregulation of typical immune cell markers, with a significant reduction of B cell (*Cd19, Cd20, BAFFR*), T cell (*Lat*) and neutrophil (*Prtn3, S100a8, S100a9*) transcripts identifying inflammatory cell infiltrates in the renal parenchyma, relative to untreated nephritic NZBW F1 kidneys. Of note, the alarmin calprotectin (*S100a8/S100a9*), exclusively downregulated by C4BP(β-) treatment, induces inflammasome activation and IL-1β-dependent monocytosis and neutrophilia.[38] Concordantly, it has been recently shown that human C4BP inhibits pancreatic islet amyloid polypeptide (IAPP)-induced inflammasome activation.[39] Indeed, the reduction/absence of both lymphoid and myeloid cells in C4BP(β-)-treated kidneys was backed by immunohistochemical evaluation and confirms that C4BP(β-) immunomodulation targets cellular effectors responsible for the immune dysregulation driving SLE.[40] Moreover, experimental and bioinformatics analyses stressed the inhibition of the pro-inflammatory NF-kB and interferon (*Irf7*) pathways through C4BP(β-)

For Peer Review Only

action, leading to suppression of innate immune responses. Both pathways have deemed essential for autoantibody production and development of nephritis in murine lupus.[41]

Chronic, unresolved inflammation in LN paves the way for ELS development, a hallmark of tissue autoimmunity, which intends to address high local concentration of autoantigens supporting the formation of a network of follicular DCs (FDCs) for antigen presentation, surrounded by proliferating/activated B- and T-cell rich areas, much like secondary lymphoid organs. It has been shown both in the NZBW F1 model and in LN patients that the chemokine CXCL13 plays an important role in the initiation and development of LN,[42,43] and abnormally increased serum CXCL13 levels could induce extensive chemotaxis of CXCR5-expressing B cells, activated T cells and DCs into renal LN tissues stimulating inflammatory ELS formation.[18,44] Conversely, it has been shown that direct CXCL13 blockade disrupts ELS formation[45] and attenuates LN in MRL-*lpr* mice.[46] Remarkably, C4BP(β-) treatment leads also to significant CXCL13 downregulation both systemically and locally in NZBW F1 kidneys. Consequently, the presence of cortical ELS in our C4BP(β-)-treated aged mice was virtually absent, consistent with substantially reduced inflammatory immune cell infiltrates compared with untreated nephritic aged mice. FDCs have been considered the main producers of CXCL13, although newly recruited monocytes, macrophages and myeloid DCs have also been shown to secrete CXCL13 in response to activation by TLR2/4 ligands.[47–51] Thus, C4BP(β-) action through the inflammatory myeloid cell-CXCL13-ELS axis would prevent ELS neogenesis in chronically inflamed tissues, which has been correlated with allograft rejection and autoimmune disease progression.[52]

In summary, additional studies will be required to further decipher the molecular mechanism of C4BP(β-) immunomodulation leading to improvement of LN pathology. Nevertheless, the relevant efficacy and specificity of C4BP(β-) in both NZBW F1 and MRL-*lpr*

For Peer Review Only

LN mice anticipates promising possibilities to explore novel therapeutic options for LN SLE patients.

For Peer Review Only

CONCISE METHODS

Proteins and drugs

Peripheral blood from healthy individuals was supplied by the local blood bank. The C4BP(β+) heterooligomer was purified from pooled plasma by $BaCl_2$ precipitation, as previously described.[53] C4BP(β-) was obtained from pooled plasma supernatants after $BaCl_2$ precipitation, and purified according to a protocol set up from Bioingenium (Barcelona, Spain). Their purity was higher than 85%, as assessed by SDS-PAGE and Coomassie Blue staining (**Supplementary Figure S6**). CYP (Genoxal®, Baxter Oncology GmbH, Halle/Westfallem, Germany), was resuspended in saline. Further information is given in Supplementary Methods.

Mice, study design and follow up

We used NZBW F1 and MRL-*lpr* female mice [54] (Jackson Laboratory, Bar Harbor, ME, USA) (6 - 8 animals/group), aged 6 months (NZBW F1 mice; 35-40 g/each) or 2.5 months (MRL-*lpr* mice; 25-30 g/each), for the studies. C4BP isoforms (C4BP(β-), rC4BP(β-), and C4BP(β+)) were administered intraperitoneally (*ip*) or subcutaneously (*sc*), as indicated, for 3 months (between 6 and 9 months of age in the case of NZBW F1 mice, and between 2.5 and 5.5 months of age in the case of MRL-*lpr* mice), at the specified doses and schedules. CYP was also administered *ip* at 2.5 mg/mouse every 10 days, in the same timeframes, as previously described.[55,56] Finally, a control group underwent vehicle PBS administration following the same administration route and schedule as the C4BP(β-) group in the different studies (**Figures 1a** and **8a; Supplementary Figures S3a** and **S4a**). Detailed procedures are given in Supplementary Methods.

Renal function analysis: proteinuria, albuminuria and BUN

For Peer Review Only

Twenty-four hour urinary protein was determined by the pyrogallol red-molibdate protein-dye binding method (Olympum Autoanalyzer AU400, Hamburg, Germany) while 24 h urinary albumin was determined using a commercially available ELISA KIT (Active motif, Carlsbad, CA, USA) according to the manufacturer's instructions.

Levels of BUN in the sera from the NZBW F1 mice were measured using a commercially available enzymatic kit (Sigma-Aldrich, St. Louis, MO, USA) according to the manufacturer's recommendations.

Assessment of anti-dsDNA antibodies

Levels of anti-dsDNA antibodies (IgG + IgA + IgM) were measured using a commercially available ELISA kit (Alpha Diagnostic International, San Antonio, TX, USA) according to the manufacturer's recommendations.

Renal histopathology

Coronal kidney slices (1–2 mm thick) were fixed in 4% paraformaldehyde and embedded in paraffin. For light microscopy, 5 μm thick tissue sections were stained with hematoxylin and eosin (H&E) and analyzed in a Nikon Eclipse 80i microscope (Nikon Instruments, Amstelveen, Netherlands). Glomerular cross-sectional area (μm^2) was calculated based on average area of 150 glomeruli in each group. Details are given in Supplementary Methods.

Immunofluorescent determination of renal IC and complement deposition

For analysis of IgG and C3 deposition, fluorescent staining of kidney cryo-sections was performed. Sections were directly stained with fluorescein isothiocyanate (FITC)-conjugated goat anti-mouse IgG (Sigma-Aldrich), and FITC-conjugated C3 (Nordic Immunology, Tilburg,

For Peer Review Only

The Netherlands). At least 10 glomeruli per section were visualized. For detailed analyses, see Supplementary Methods.

Complement activity assay

Activity of the classical complement pathway in fresh sera was determined by C3b deposition on K562 cells opsonized with rabbit polyclonal antibodies (Agrisera, Vännäs, Sweden), as previously described,[20] and quantified using FITC-conjugated goat IgG fraction to mouse complement C3 antibody (MP Biomedicals, Solon, OH, USA) and flow cytometry. Heat-inactivated serum samples (56 ºC, 30 min) were used as negative controls. A further description is given in Supplementary Methods.

Immunohistochemistry

The following primary antibodies were used: polyclonal rabbit anti-mouse CD11c (1:200, Biorbyt, BioNova, Cambridge, UK), polyclonal rabbit anti-mouse Lat (1:50, ThermoFisher, Waltham, MA, USA), monoclonal rat anti-mouse Gr1 (1:50, R&D Systems, Minneapolis, MN, USA), monoclonal rat anti-mouse F4/80 (1:50, ThermoFischer), monoclonal rat anti-mouse CD19 (1:200, ThermoFischer). F4/80 marker detection required antigen retrieval using proteinase K. After PBS washing, slices were incubated with the appropriate secondary antibody: biotinylated goat anti-rabbit IgG (1:200, Vector laboratories, Peterborough, UK), or ImmPRESS™ HRP anti-rat IgG (mouse adsorbed) polymer detection kit (Vector laboratories) for 1 h at RT. Regarding CD11c and Lat markers, standard Vectastain (ABC) avidin-biotin peroxidase complex (Vector laboratories) was applied. For further details about tissue processing and staining, see Supplementary Methods.

TUNEL Assay

For Peer Review Only

Apoptosis detection was performed by terminal deoxynucleotidyl transferase-mediated dUTP nick-end labeling (TUNEL) using the "TACS TdT *in situ* DAB" kit (R&D Systems) according to the manufacturer's instructions. Details are given in Supplementary Methods.

Differential gene expression analysis

Total RNA from mouse kidneys was extracted using the RNeasy Mini Kit (Qiagen, Hilden, Germany). Gene expression profiling was performed by interrogating reverse transcribed pooled cDNA (2-3 animals/group) using custom TaqMan Low Density Arrays (TLDA Cards) (Applied Biosystems, Carlsbad, CA, USA) (**Supplementary Table S1)** run on the 7900HT system for quantitative real-time PCR analysis according to the manufacturer's instructions. Differentially expressed genes were analyzed using the Ingenuity Pathway Analysis (IPA) (Ingenuity Systems, Qiagen) to identify biological and molecular networks differentially regulated in the LN model. Selected gene transcripts were further validated in individual mouse kidney samples by RT-qPCR using TaqMan Gene Expression Assays (Applied BioSystems). Pathway annotation of the RT-qPCR-validated gene set was performed through PathwAX.[57] Detailed procedures are given in Supplementary Methods.

Mouse cytokine array

Serum and renal lysates were analyzed using the Proteome Profiler Array "Mouse Cytokine Array Panel A" kit (R&D Systems), according to the manufacturer's instructions. Further details are given in Supplementary Methods.

CXCL13 ELISA

For Peer Review Only

CXCL13 cytokine levels from both sera and tissue lysates were quantified using the "Legend Max Mouse CXCL13 (BLC) ELISA" kit (BioLegend, San Diego, CA, USA) according to the manufacturers' instructions.

Statistical analysis

Statistical analyses and scientific graphing were performed using the GraphPad Prism 6 software (GraphPad software, Inc, La Jolla, CA, USA). Two-way ANOVA, corrected for multiple comparisons using the Holm-Sidak method, was applied to analyze proteinuria, albuminuria, BUN, anti-dsDNA antibodies, complement activity and dermatitis scores throughout the follow up studies. One-way ANOVA, corrected for multiple comparisons using the Dunnett's method, was employed to assess histological data and CXCL13 cytokine levels. Meier plots along with the log-rank (Mantel-Cox) test were performed to assess the differences in the survival distributions. Vehicle PBS-treated mice were assigned as the reference group, unless otherwise indicated. Relative gene expression levels between the C4BP(β-)- and CYP-treatment groups relative to the vehicle PBS-treated group in the validation step were analyzed using the one sample t-test. The Friedman test, corrected using the Dunn's post-hoc analysis method, was applied to compare flow cytometry (MFI) data. Unless otherwise stated, data are expressed as mean values ± SD. In all cases, a P value < 0.05 was considered significant.

For Peer Review Only

SUPPLEMENTARY MATERIAL

Supplementary material is linked to the online version of the paper at www.kidney-international.org.

For Peer Review Only

DISCLOSURE

JMA is co-inventor on pending or issued patents involving compounds and methods for immunomodulation. The authors report no other conflicts of interest in this work.

For Peer Review Only

ACKNOWLEDGEMENTS

We thank Nuria Lluch and Jordi Ortiz (Spherium Biomed S.L.) for fruitful discussions and contribution to the research. This work was supported by the Ministerio de Ciencia, Innovación y Universidades (Madrid, Spain) (grants FIS-ISCIII PI16/00377 and PI13/00969, cofunded by FEDER funds/European Regional Development Fund (ERDF)-a way to build Europe-), the Generalitat de Catalunya (grant 2017SGR291, and CERCA Program), and Spherium Biomed S.L. Drs. Aran and Rodriguez de Córdoba are members of the Red de Excelencia "Complemento en salud y enfermedad" (SAF2016-81876-REDT). Dr. Rodriguez de Córdoba is supported by the Spanish "Ministerio de Economía y Competitividad/FEDER" [SAF2015-66287-R] and the Autonomous Region of Madrid [S2017/BMD-3673]. Dr. Aran is sponsored by the "Researchers Consolidation Program" from the SNS-Dpt. Salut Generalitat de Catalunya (Exp. CES06/012).

For Peer Review Only

REFERENCES

1. Maroz N, Segal MS. Lupus nephritis and end-stage kidney disease. *Am J Med Sci*. 2013;346:319-323.
2. Monteith AJ, Kang S, Scott E, et al. Defects in lysosomal maturation facilitate the activation of innate sensors in systemic lupus erythematosus. *Proc Natl Acad Sci U S A*. 2016;113:E2142-51.
3. Kang S, Fedoriw Y, Brenneman EK, et al. BAFF induces tertiary lymphoid structures and positions T cells within the glomeruli during lupus nephritis. *J Immunol*. 2017;198:2602-2611.
4. Das A, Heesters BA, Bialas A, et al. Follicular dendritic cell activation by TLR ligands promotes autoreactive B cell responses. *Immunity*. 2017;46:106-119.
5. Krieg AM. The toll of too much TLR7. *Immunity*. 2007;27:695-697.
6. Chang A, Henderson SG, Brandt D, et al. In situ B cell-mediated immune responses and tubulointerstitial inflammation in human lupus nephritis. *J Immunol*. 2011;186:1849-1860.
7. Venuturupalli S. Rethinking biologics in lupus nephritis. *Lupus*. 2016;25:1102-1110.
8. Sánchez-Corral P, Criado García O, Rodríguez de Córdoba S. Isoforms of human C4b-binding protein. I. Molecular basis for the C4BP isoform pattern and its variations in human plasma. *J Immunol*. 1995;155:4030-4036.
9. Criado García O, Sánchez-Corral P, Rodríguez de Córdoba S. Isoforms of human C4b-binding protein. II. Differential modulation of the C4BPA and C4BPB genes by acute phase cytokines. *J Immunol*. 1995;155:4037-4043.
10. Blom AM. Structural and functional studies of complement inhibitor C4b-binding protein. *Biochem Soc Trans*. 2002;30:978-982.
11. Dahlbäck B. Protein S and C4b-binding protein: components involved in the regulation of the protein C anticoagulant system. *Thromb Haemost*. 1991;66:49-61.

For Peer Review Only

12. Kask L, Trouw LA, Dahlbäck B, et al. The C4b-binding protein-protein S complex inhibits the phagocytosis of apoptotic cells. *J Biol Chem*. 2004;279:23869-23873.

13. Olivar R, Luque A, Naranjo-Gómez M, et al. The α7β0 isoform of the complement regulator C4b-binding protein induces a semimature, anti-inflammatory state in dendritic cells. *J Immunol*. 2013;190:2857-2872.

14. Wu Y, Tang W, Zuo J. Toll-like receptors: potential targets for lupus treatment. *Acta Pharmacol Sin*. 2015;36:1395-1407.

15. Schellekens H. Immunogenicity of therapeutic proteins: Clinical implications and future prospects. *Clin Ther*. 2002;24:1720-1740.

16. Sugisaki T, Takase S. Composition of immune deposits present in glomeruli of NZB/W F1 mice. *Clin Immunol Immunopathol*. 1991;61:296-308.

17. Kang S, Rogers JL, Monteith AJ, et al. Apoptotic debris accumulates on hematopoietic cells and promotes disease in murine and human systemic lupus erythematosus. *J Immunol*. 2016;196:4030-4039.

18. Ishikawa S, Sato T, Abe M, et al. Aberrant high expression of B lymphocyte chemokine (BLC/CXCL13) by C11b+CD11c+ dendritic cells in murine lupus and preferential chemotaxis of B1 cells towards BLC. *J Exp Med*. 2001;193:1393-1402.

19. Fritchen C, Kim HJ, Lightfoot RW. Studies of murine complement. Correlation of hypocomplementemia with other disease parameters in individual NZB/W mice and demonstration of anti-complementary material. *Arthritis Rheum*. 1980;23:904-910.

20. Blom AM, Nandakumar KS, Holmdahl R. C4b-binding protein (C4BP) inhibits development of experimental arthritis in mice. *Ann Rheum Dis*. 2009;68:136-142.

21. Wang Y, Hu Q, Madri JA, et al. Amelioration of lupus-like autoimmune disease in NZB/WF1 mice after treatment with a blocking monoclonal antibody specific for complement component C5. *Proc Natl Acad Sci U S A*. 1996;93:8563-8568.

For Peer Review Only

22. Bao L, Osawe I, Haas M, et al. Signaling through up-regulated C3a receptor is key to the development of experimental lupus nephritis. *J Immunol*. 2005;175:1947-1955.

23. Bao L, Osawe I, Puri T, et al. C5a promotes development of experimental lupus nephritis which can be blocked with a specific receptor antagonist. *Eur J Immunol*. 2005;35:2496-2506.

24. Song H, He C, Knaak C, et al. Complement receptor 2-mediated targeting of complement inhibitors to sites of complement activation. *J Clin Invest*. 2003;111:1875-1885.

25. Bao L, Haas M, Kraus DM, et al. Administration of a soluble recombinant complement C3 inhibitor protects against renal disease in MRL/lpr mice. *J Am Soc Nephrol*. 2003;14:670-679.

26. Sekine H, Kinser TTH, Qiao F, et al. The benefit of targeted and selective inhibition of the alternative complement pathway for modulating autoimmunity and renal disease in MRL/lpr mice. *Arthritis Rheum*. 2011;63:1076-1085.

27. Jacob CO, Pricop L, Putterman C, et al. Paucity of clinical disease despite serological autoimmunity and kidney pathology in lupus-prone New Zealand mixed 2328 mice deficient in BAFF. *J Immunol*. 2006;177:2671-2680.

28. Ramanujam M, Wang X, Huang W, et al. Similarities and differences between selective and nonselective BAFF blockade in murine SLE. *J Clin Invest*. 2006;116:724-734.

29. Bergtold A, Gavhane A, D'Agati V, et al. FcR-bearing myeloid cells are responsible for triggering murine lupus nephritis. *J Immunol*. 2006;177:7287-7295.

30. Zampeli E, Klinman DM, Gershwin ME, et al. A comprehensive evaluation for the treatment of lupus nephritis. *J Autoimmun*. 2017;78:1-10.

31. de Córdoba SR, Pérez-Blas M, Ramos-Ruiz R, et al. The gene coding for the β-chain of C4b-binding protein (C4BPB) has become a pseudogene in the mouse. *Genomics*. 1994;21:501-509.

For Peer Review Only

32. Kristensen T, Ogata RT, Chung LP, et al. cDNA structure of murine C4b-binding protein, a regulatory component of the serum complement system. *Biochemistry*. 1987;26:4668-4674.

33. Wenderfer SE, Soimo K, Wetsel RA, et al. Analysis of C4 and the C4 binding protein in the MRL/lpr mouse. *Arthritis Res Ther*. 2007;9:R114.

34. Olivar R, Luque A, Cárdenas-Brito S, et al. The complement inhibitor Factor H generates an anti-inflammatory and tolerogenic state in monocyte-derived dendritic cells. *J Immunol*. 2016;196:4274-4290.

35. Veglia F, Perego M, Gabrilovich D. Myeloid-derived suppressor cells coming of age. *Nat Immunol*. 2018;19:108-119.

36. Sendo S, Saegusa J, Morinobu A. Myeloid-derived suppressor cells in non-neoplastic inflamed organs. *Inflamm Regen*. 2018;38:19.

37. Celhar T, Hopkins R, Thornhill SI, et al. RNA sensing by conventional dendritic cells is central to the development of lupus nephritis. *Proc Natl Acad Sci U S A*. 2015;112:E6195-204.

38. Nagareddy PR, Kraakman M, Masters SL, et al. Adipose tissue macrophages promote myelopoiesis and monocytosis in obesity. *Cell Metab*. 2014;19:821-835.

39. Kulak K, Westermark GT, Papac-Milicevic N, et al. The human serum protein C4b-binding protein inhibits pancreatic IAPP-induced inflammasome activation. *Diabetologia*. 2017;60:1522-1533.

40. Moulton VR, Suarez-Fueyo A, Meidan E, et al. Pathogenesis of human systemic lupus erythematosus: a cellular perspective. *Trends Mol Med*. 2017;23:615-635.

41. Miyagawa F, Tagaya Y, Ozato K, et al. Essential requirement for IFN regulatory factor 7 in autoantibody production but not development of nephritis in murine lupus. *J Immunol*. 2016;197:2167-2176.

For Peer Review Only

42. Schiffer L, Bethunaickan R, Ramanujam M, et al. Activated renal macrophages are markers of disease onset and disease remission in lupus nephritis. *J Immunol*. 2008;180:1938-1947.

43. Sang A, Zheng Y-Y, Morel L. Contributions of B cells to lupus pathogenesis. *Mol Immunol*. 2014;62:329-338.

44. He DN, Chen WL, Long KX, et al. Association of serum CXCL13 with intrarenal ectopic lymphoid tissue formation in lupus nephritis. *J Immunol Res*. 2016;2016:4832543.

45. Yamamoto K, Nishiumi S, Yang L, et al. Anti-CXCL13 antibody can inhibit the formation of gastric lymphoid follicles induced by Helicobacter infection. *Mucosal Immunol*. 2014;7:1244-1254.

46. Wu X, Guo J, Ding R, et al. CXCL13 blockade attenuates lupus nephritis of MRL/lpr mice. *Acta Histochem*. 2015;117:732-737.

47. Carlsen HS, Baekkevold ES, Morton HC, et al. Monocyte-like and mature macrophages produce CXCL13 (B cell-attracting chemokine 1) in inflammatory lesions with lymphoid neogenesis. *Blood*. 2004;104:3021-3027.

48. Vermi W, Facchetti F, Riboldi E, et al. Role of dendritic cell-derived CXCL13 in the pathogenesis of Bartonella henselae B-rich granuloma. *Blood*. 2006;107:454-462.

49. Rupprecht TA, Kirschning CJ, Popp B, et al. Borrelia garinii induces CXCL13 production in human monocytes through Toll-like receptor 2. *Infect Immun*. 2007;75:4351-4356.

50. Moreth K, Brodbeck R, Babelova A, et al. The proteoglycan biglycan regulates expression of the B cell chemoattractant CXCL13 and aggravates murine lupus nephritis. *J Clin Invest*. 2010;120:4251-4272.

51. Cohen SB, Smith NL, McDougal C, et al. Beta-catenin signaling drives differentiation and proinflammatory function of IRF8-dependent dendritic cells. *J Immunol*. 2015;194:210-222.

For Peer Review Only

52. Neyt K, Perros F, GeurtsvanKessel CH, et al. Tertiary lymphoid organs in infection and autoimmunity. *Trends Immunol*. 2012;33:297-305.

53. Mohlin FC, Blom AM. Purification and functional characterization of C4b-binding protein (C4BP). *Methods Mol Biol*. 2014;1100:169-176.

54. Rottman JB, Willis CR. Mouse models of systemic lupus erythematosus reveal a complex pathogenesis. *Vet Pathol*. 2010;47:664-676.

55. Alperovich G, Rama I, Lloberas N, et al. New immunosuppresor strategies in the treatment of murine lupus nephritis. *Lupus*. 2007;16:18-24.

56. Ripoll È, Merino A, Goma M, et al. CD40 gene silencing reduces the progression of experimental lupus nephritis modulating local milieu and systemic mechanisms. *PLoS One*. 2013;8:e65068.

57. Ogris C, Helleday T, Sonnhammer ELL. PathwAX: a web server for network crosstalk based pathway annotation. *Nucleic Acids Res*. 2016;44:W105-W109.

For Peer Review Only

FIGURE CAPTIONS

Figure 1.- Renal function determination in lupus-prone NZBW F1 mice.

Schematic administration schedule and dosage for intraperitoneal (*ip*) injection of C4BP(β-) and vehicle (PBS) (blue arrows), and cyclophosphamide (CYP) (red arrows) in lupus-prone NZBW F1 mice (**a**). Proteinuria and albuminuria were monitored monthly over the course of the assay and all animals were sacrificed at week 36 (w36). Total 24-h urinary protein was determined by Pyrogallol Red-molybdate protein dye-binding assay (**b**), and 24-h urinary albumin was determined by ELISA (**c**) as described in Methods. Data are normalized by mouse weight and expressed as mean values ± SD (n= 4-8 mice/group); ***$p < 0.001$; ****$p < 0.000,1$ compared with control, PBS-treated mice.

Figure 2.- Anti-dsDNA autoantibody production and renal histology assessment in lupus-prone NZBW F1 mice.

(**a**) Serum levels of anti-dsDNA antibodies correlating with disease activity were measured by ELISA from week 20 (pretreatment) to week 36. Data are expressed as mean ± SD (n= 7 mice/group); *$p < 0.05$; **$p < 0.01$; ****$p < 0.0001$, compared with vehicle PBS-treated mice. (**b**) Representative sections of renal cortex from 36-week old NZBW F1 mice treated with CYP (left), C4BP(β-) (center) and vehicle PBS (right) mice stained with hematoxylin and eosin. Images are shown at low (upper panels; scale bars: 200 μm) and high (lower panels; scale bars: 50 μm) magnification. The data obtained were used to comparatively evaluate the glomeruli area (**c**) and to semi-quantitatively grade histopathology traits indicating active LN (mesangial expansion, endocapillary proliferation, glomerular deposits, extracapillary proliferation and interstitial infiltrates), as well as chronic lesions (tubular atrophy and interstitial fibrosis) (**d**).

For Peer Review Only

Figure 3.- Immunohistochemical analysis of IgG and C3 deposits and evaluation of apoptosis in the renal cortex of lupus-prone NZBW F1 mice.

For analysis of local IgG and C3 deposition, fluorescent staining of renal cryo-sections was performed (**a**). Representative fluorescent images from IgG- and C3-stained vehicle PBS- and C4BP(β-)-treated NZBW F1 mice are shown (scale bar: 50 μm) (upper panels). Fluorescence was expressed as mean fluorescence intensity (MFI) ± SD (n= 7 mice/group); ****$p < 0.0001$, compared with vehicle PBS mice (lower panels). Apoptosis in the renal cortex was detected by TUNEL assay (**b**). Representative images from renal cortex of CYP-, C4BP(β-)-, and PBS vehicle-treated NZBW F1 mice are shown at low (scale bar: 200 μm) and high (scale bar: 50 μm) magnification. Scoring of cortical apoptotic cells as cell number per field (left graph) and glomerular apoptotic cells as cell number per glomerular cut section (*gcs*) (right graph). Data are expressed as mean ± SD (n= 3 mice/group); ****p <0.0001, compared with vehicle PBS-treated mice.

Figure 4.- Comparative transcriptional profiling of renal tissue from lupus-prone NZBW F1 mice.

Overall comparative transcriptional profiles of 36-week renal tissue from CYP- and C4BP(β-)-treated mice relative to the 36-week nephritic transcriptional profile displayed by renal tissue from vehicle PBS-treated mice (**a**). Total renal RNA was interrogated against a panel of 377 murine genes relevant in LN pathology. Gene expression data are given as Log_2FC (FC, fold change). The discontinuous horizontal lines indicate a fold change threshold of ± 1.8 for upregulated and downregulated genes. *TaqMan* RT-qPCR individual validation of all genes showing a FC induction ≥ 2 in the C4BP(β-) transcriptional profile (**b**). Relative expression data for the specified genes was obtained from renal RNA of individual mice belonging to each

For Peer Review Only

treatment group (n= 3-5 mice/group). Log_2FC values are expressed as mean ± SD; **p* <0.05, ***p* <0.01 compared with vehicle PBS-treated mice.

Figure 5.- Circulating and renal cytokine profile from lupus-prone NZBW F1 mice.

Sera (**a**) and renal tissue extracts (**c**) were incubated with the R&D Systems "Proteome Profiler Mouse Cytokine Array Kit", according to the manufacturer's guidelines. The density of each dot was quantified with Quantity One® software and displayed as normalized mean pixel density for each relevant cytokine and treatment. Additional validation of the chemokine CXCL13 was performed in individual mouse samples (n= 4 mice/group) by a specific ELISA (**b** and **d**). Data are expressed as mean values ± SD; *****p* <0.0001, compared with vehicle PBS-treated mice.

Figure 6.- Immunohistochemistry of renal cortex from lupus-prone NZBW F1 mice.

Assessment of immune cell infiltrates in renal cortex sections from CYP-, C4BP (β-)-, and vehicle PBS-treated aged NZBW F1 mice at the end of the study (36 weeks old). Local intense perivascular, periglomerular and/or glomerular staining was observed in vehicle PBS-treated kidneys surveyed for activated T cells (Lat), B cells (CD19), and myeloid cells such as neutrophils (Gr1), DCs (CD11c), and monocytes/macrophages (F4/80), the latter presenting a strong and diffuse periglomerular staining (lower panels). Conversely, CYP-treated (upper panels) and C4BP(β-)-treated (middle panels) kidneys were found scarcely stained for the above-referred inflammatory markers. Scale bars: 50 μm. Results from each panel are representative of staining performed on tissue from 3 animals in each group.

Figure 7.- C4BP(β-) treatment prevents the development of ELS in lupus-prone NZBW F1 mice.

For Peer Review Only

Upper panels, low resolution hematoxilin-eosin stained representative renal cortex sections from C4BP(β-)-treated (left) and vehicle PBS-treated (right) aged (36 week old) NZBW F1 mice. ELS are clearly visible in the PBS-treated mice (black arrows), but absent in C4BP(β-)-treated mice. Scale bars: 200 μm (representative images from 4 mice/group). Lower panels, consecutive renal sections of C4BP(β-)-treated and PBS-treated mice stained with hematoxilin-eosin (left), and immunostained with Lat (activated T cell marker) (center) and CD19 (B cell marker) (right). Note the co-localization of T and B cells within a well-developed ELS surrounding an arteriole (a) and next to a vein (v) in the higher magnification images from PBS-treated renal cortex. ELS are virtually nonexistent in C4BP(β-)-treated renal cortex. Scale bars: 100 μm.

Figure 8.- C4BP(β-) attenuates autoimmune lupus manifestations in MRL/lpr mice.

(a) Schematic administration schedule and dosage for intraperitoneal (*ip*) injection of C4BP(β-) and vehicle (PBS) (blue arrows), and cyclophosphamide (CYP) (red arrows) in MRL/lpr mice. (**b**) Proteinuria was monitored bimonthly (unless otherwise stated) over the course of the assay from week 9 until week 22. Total 24-h urinary protein was determined by Pyrogallol Red-molybdate protein dye-binding assay. Data are normalized by mouse weight and expressed as cumulative mean values (PBS, n= 8; C4BP(β-) and CYP, n= 6); $*p < 0.05$; $**p < 0.01$ compared with control, PBS-treated mice. (**c**) Kaplan-Meier survival curves from lupus-prone MRL/lpr mice. Cumulative survival curves showed 100% survival (8/8) in the CYP-treated and C4BP(β-)-treated mice, and 62.5% survival (5/8) in PBS-treated mice at the end of the study (day 147). Red arrows identify the start (day 70) and the end (day 147) of the treatment period. n=6-8 mice/group; $*p < 0.05$, compared with vehicle PBS-treated mice; long-rank test. **(d)** Representative sections of renal cortex from 22-week old MRL/lpr mice treated with CYP (left), C4BP(β-) (center) and vehicle PBS (right) mice stained with hematoxylin and eosin. Images are shown at 200 μm magnification. The data obtained were used to semi-quantitatively grade

For Peer Review Only

histopathology traits indicating active LN (mesangial expansion, endocapillary proliferation, glomerular deposits, extracapillary proliferation and interstitial infiltrates), as well as chronic lesions (tubular atrophy and interstitial fibrosis) (n= 3 mice/group) **(e)** Clinical features of dermatitis in MRL-lpr mice treated with C4BP(β-) (*left panels*) or PBS (*right panels*). Major lesions were observed around the facial and scapular regions, and vasculitis was evident in the ears of PBS-treated mice. Skin lesion severity score at weeks 19 and 21 for each of the study groups is shown on the right (PBS, n= 5; C4BP(β-) and CYP, n= 6); *$p < 0.05$; **$p < 0.01$ compared with PBS-treated mice.

For Peer Review Only

Table 1.- Pathway annotation of NZBW F1 renal genes downregulated by C4BP(β-) treatment based on network crosstalk (PathwAX).

Pathway class	#	Relevant pathway	FWER	Network connectivity of C4BP(β-)-induced genes (Links)							
				Ms4a1	Prtn3	Tnfrsf13c	Lat	Cd19	S100a8	S100a9	Irf7
Human diseases	14	Systemic lupus erythematosus	$2.20x10^{-3}$	5	1						1
Organismal systems	2	Hematopoietic cell lineage	$1.53x10^{-14}$	4		1	4	4			
	3	B cell receptor signaling pathway	$1.68x10^{-12}$	3		2	3				1
	15	Antigen processing and presentation	$2.46x10^{-3}$	5	1		1				
	18	T cell receptor signaling pathway	$6.01x10^{-3}$	1			7				
Environmental information Processing	4	NF-kappa B signaling pathway	$2.27x10^{-9}$	3			5	2		1	1
	6	Cell adhesion molecules (CAMs)	$2.44x10^{-6}$	7			2	1			
	12	Cytokine-cytokine receptor interaction	$9.62x10^{-4}$	4				2			1

Green boxes represent query genes linked to the pathway; Purple boxes indicate genes which are part of the pathway. Darker shades indicate higher connectivity.
FWER: Family-Wise Error Rate.
#: Order number. The results are sorted by increasing FWER.

For Peer Review Only

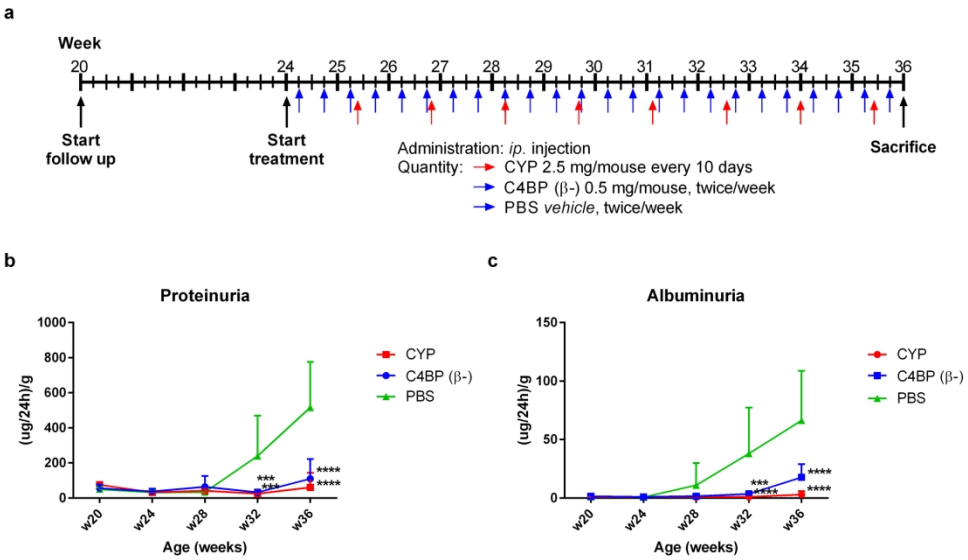

Figure 1

189x113mm (300 x 300 DPI)

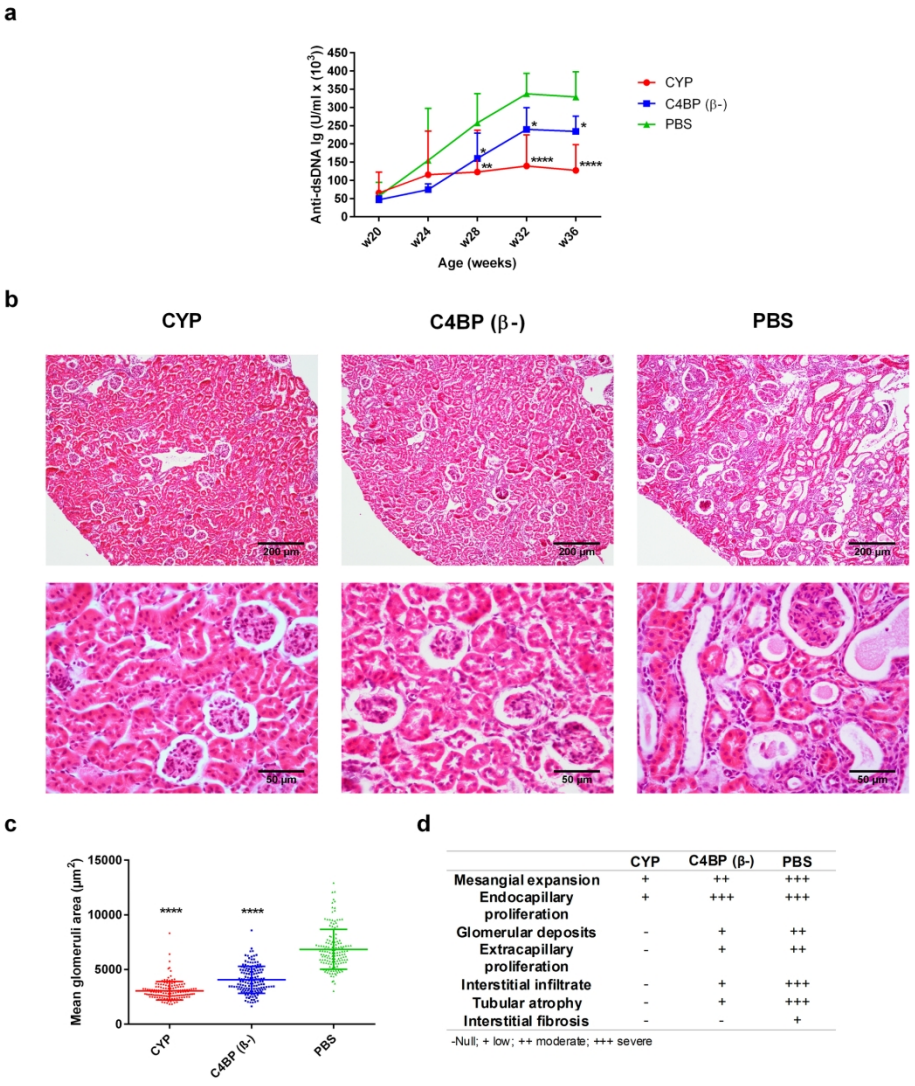

	CYP	C4BP (β-)	PBS
Mesangial expansion	+	++	+++
Endocapillary proliferation	+	+++	+++
Glomerular deposits	-	+	++
Extracapillary proliferation	-	+	++
Interstitial infiltrate	-	+	+++
Tubular atrophy	-	+	+++
Interstitial fibrosis	-	-	+

-Null; + low; ++ moderate; +++ severe

Figure 2

189x214mm (300 x 300 DPI)

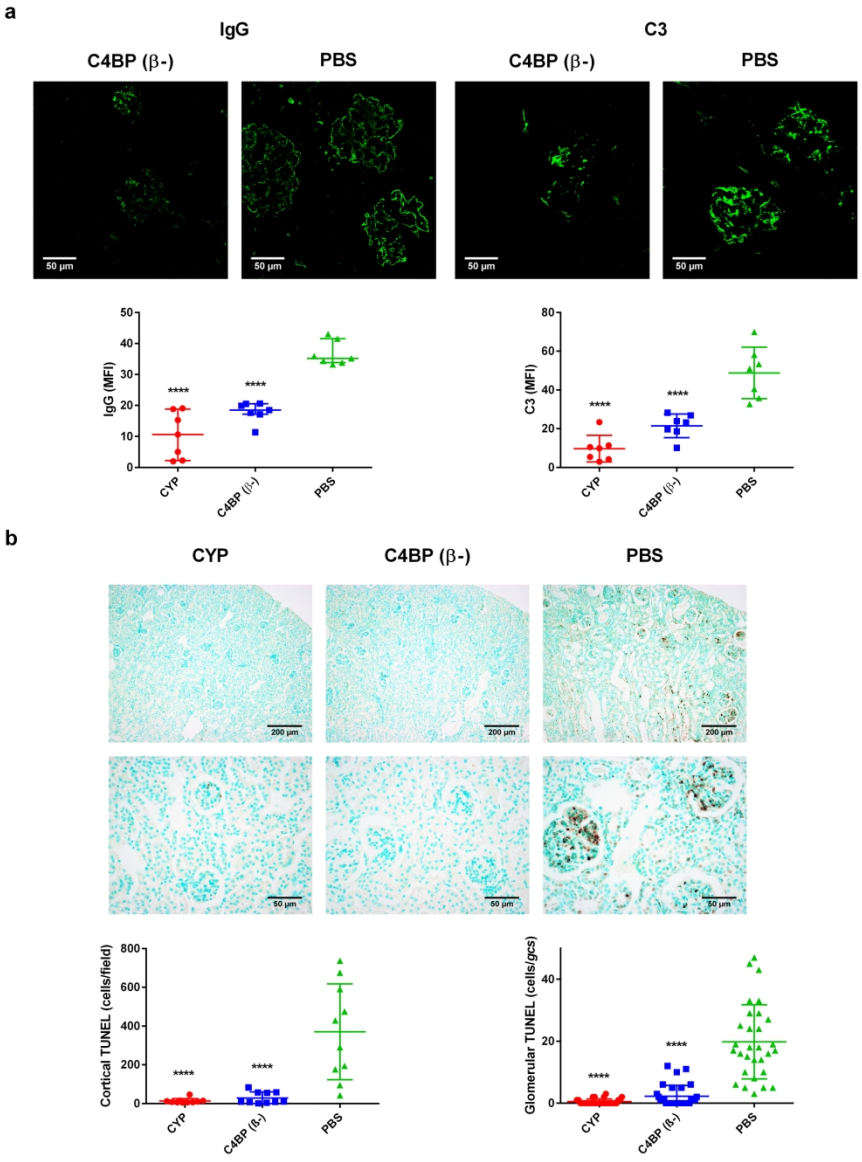

Figure 3

189x257mm (300 x 300 DPI)

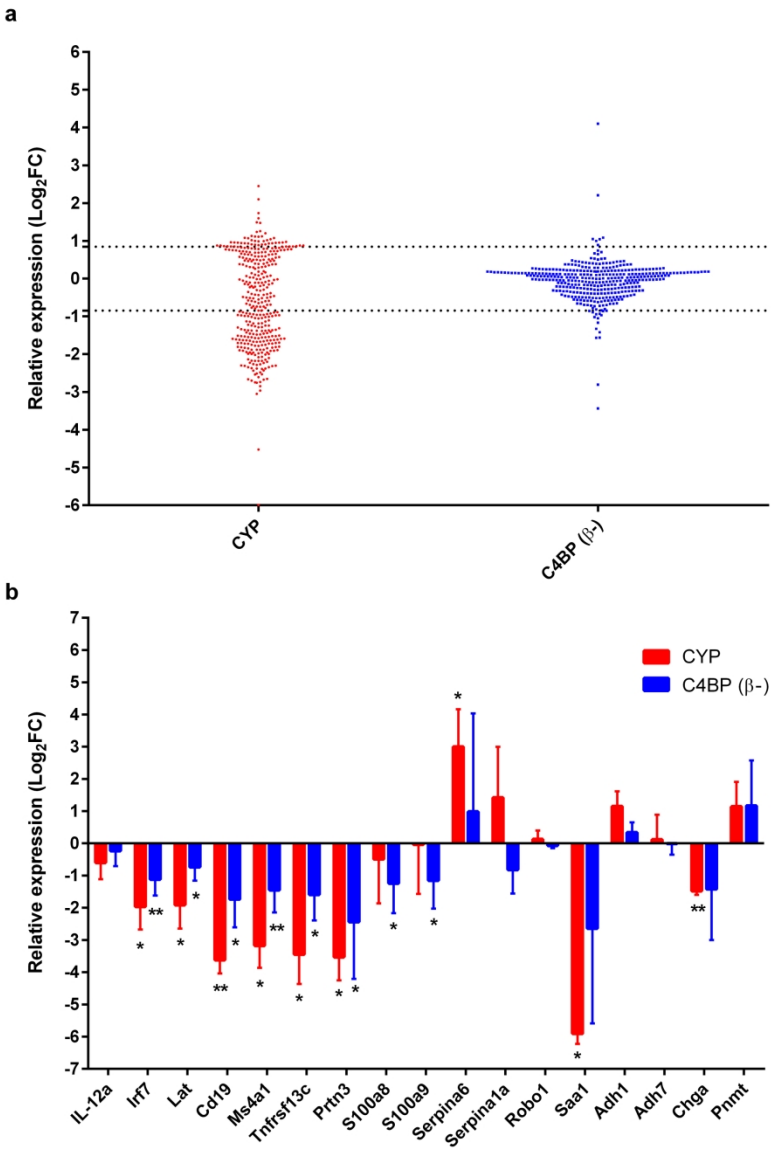

Figure 4

189x279mm (300 x 300 DPI)

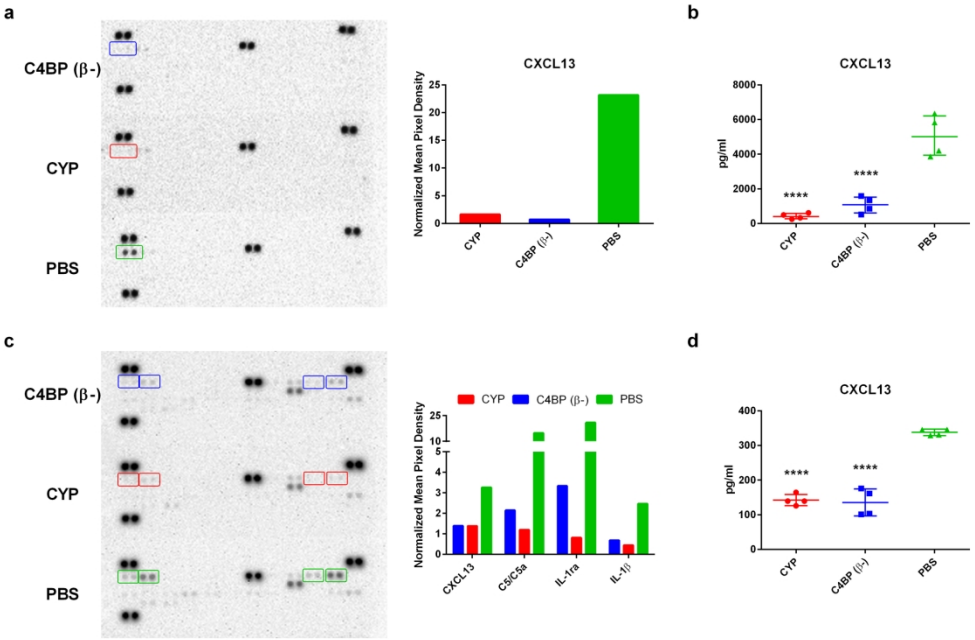

Figure 5

189x126mm (300 x 300 DPI)

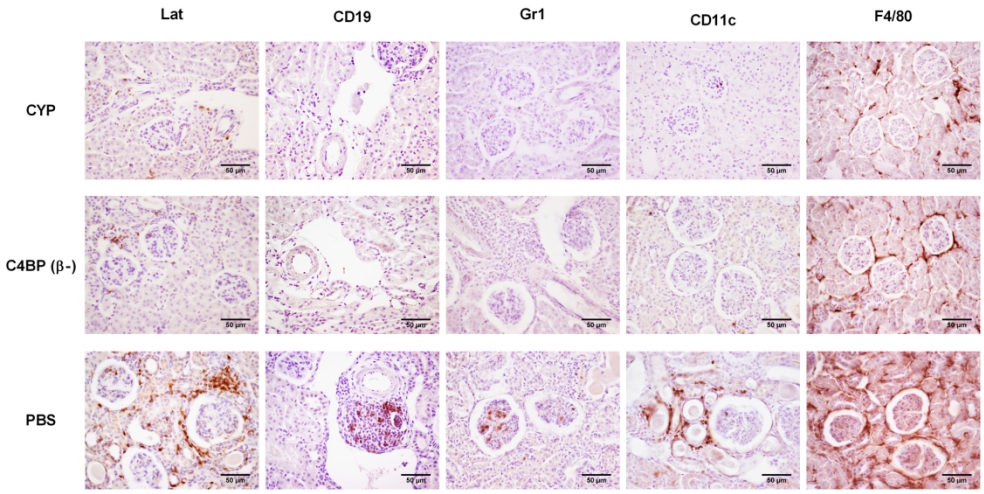

Figure 6

189x96mm (300 x 300 DPI)

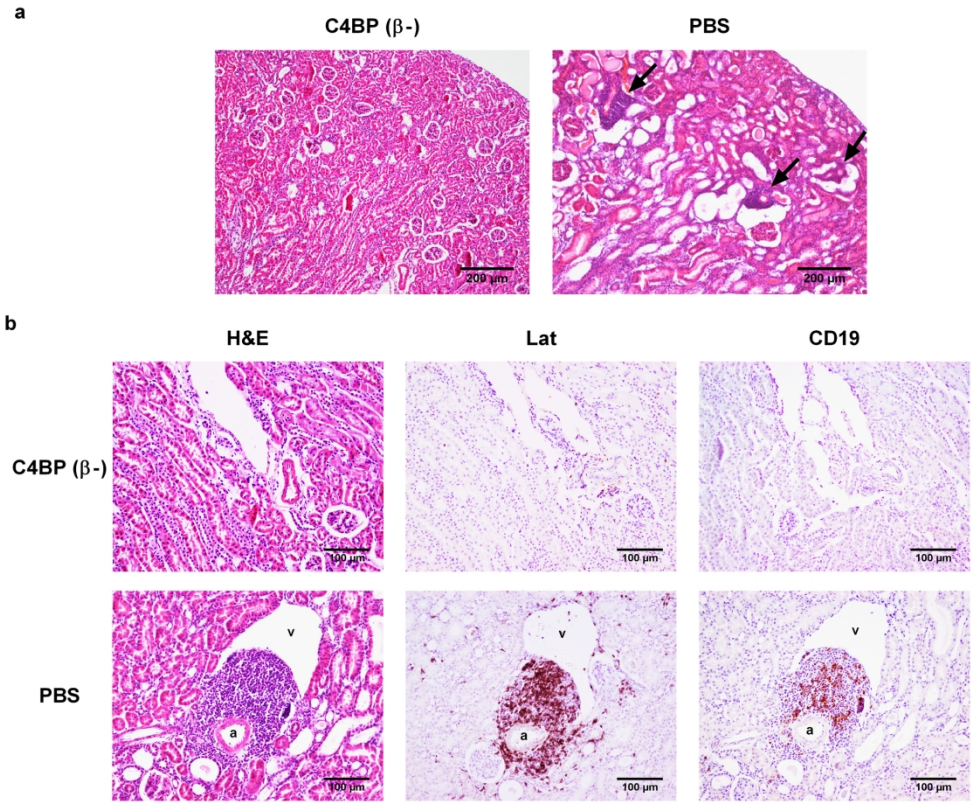

Figure 7

189x158mm (300 x 300 DPI)

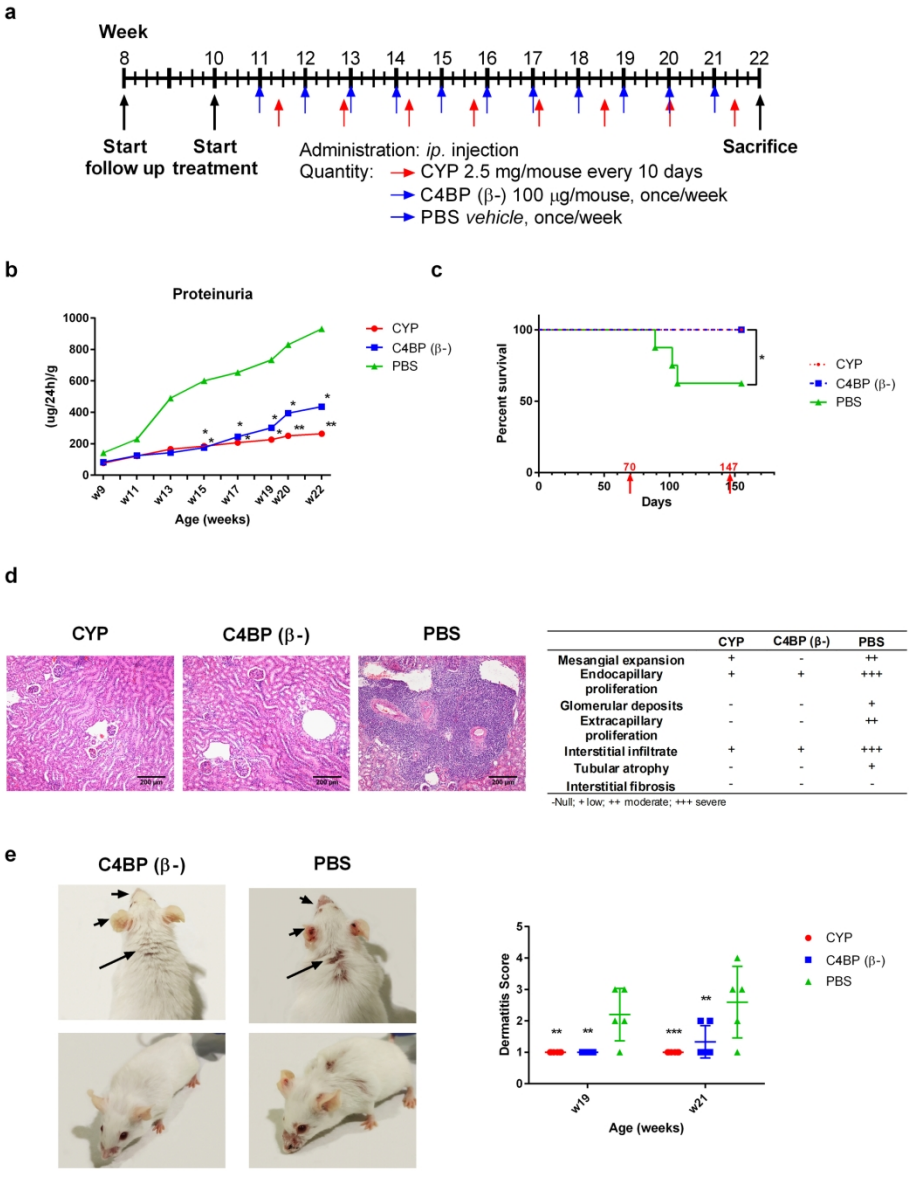

	CYP	C4BP (β-)	PBS
Mesangial expansion	+	-	++
Endocapillary proliferation	+	+	+++
Glomerular deposits	-	-	+
Extracapillary proliferation	-	-	++
Interstitial infiltrate	+	+	+++
Tubular atrophy	-	-	+
Interstitial fibrosis	-	-	-

-Null; + low; ++ moderate; +++ severe

Figure 8

189x243mm (300 x 300 DPI)

Luque et al. (September 2019) KI-12-18-1865

SUPPLEMENTARY FIGURE CAPTIONS

Supplementary Figure S1.- Human C4BP(β-) down-regulates CD80 and CD86 co-stimulatory molecules in mouse BMDCs stimulated through the TLR7 agonist gardiquimod. Mouse BMDCs, generated as described in *Supplementary Methods*, were incubated throughout their differentiation and maturation process with 5 μg/ml of human C4BP(β-). BMDC maturation was achieved by gardiquimod treatment (10 μg/ml). Cells were then collected, washed, and analyzed by flow cytometry for cell surface expression of CD80 and CD86 surface markers. (**a**) Histograms from one representative experiment are shown. The MFIs for the cell surface markers are indicated in each histogram. (**b**) MFI for CD80 and CD86 cell surface markers. iDC, untreated, immature BMDCs; mDC, untreated, gardiquimod-matured BMDCs; C4BP(β-), C4BP(β-)-treated, gardiquimod-matured BMDCs. The results shown are the median +/- IQR from 3 independent experiments (*$p < 0.05$ compared to mDC).

Supplementary Figure S2.- Time-course of anti-human C4BP(β-) antibody development in lupus-prone NZBWF1 mice. Serum levels of anti-human C4BP(β-) antibody production were measured by ELISA from week 20 (pretreatment) to week 36. The anti-human C4BP(β-) antibody titer increased progressively with the time in the C4BP(β-)-treated mice. Cyclophosphamide (CYP), used as a negative control group, did not develop anti-human C4BP(β-)-specific antibodies at any time of the study period. Data are expressed as mean O.D. (450 nm) ± SD (n= 6 mice/group). ****$p < 0.0001$ compared with CYP-treated mice.

Supplementary Figure S3.- Renal function determination in lupus-prone NZBW F1 mice after subcutaneous administration low-dose rC4BP(β-). (**a**) Schematic administration

For Peer Review Only

schedule and dosage for subcutaneous (*sc*) injection of C4BP(β-) and vehicle (PBS) (blue arrows), and cyclophosphamide (CYP) (red arrows) in NZBW F1 mice. (**b**) Unless otherwise indicated, proteinuria was monitored monthly over the course of the assay until week 37. Total 24-h urinary protein was determined by Pyrogallol Red-molybdate protein dye-binding assay. Data are normalized by mouse weight and expressed as mean values ± SD (n= 6 mice/group); *$p < 0.05$; ***$p < 0.001$; ****$p < 0.0001$ compared with control, PBS-treated mice. (**c**) Time-course of anti-human rC4BP(β-) antibody development from rC4BP(β-)-treated NZBWF1 mice. Serum levels of anti-human rC4BP(β-) antibody production were measured by ELISA from week 21 (pretreatment) to week 37. The anti-human rC4BP(β-) antibody titer increased progressively with the time in the rC4BP(β-)-treated mice. Cyclophosphamide (CYP), used as a negative control group, did not develop anti-human rC4BP(β-)-specific antibodies at any time of the study period. Data are expressed as mean O.D. (450 nm) ± SD (n= 6 mice/group). ****$p < 0.0001$ compared with CYP-treated mice. (**d**) Kaplan-Meier survival curves from lupus-prone NZBWF1 mice. Cumulative survival curves showed 100% survival in the CYP-treated mice (6/6), and 67% survival (4/6) in C4BP(β-)-treated mice at the end of the study (day 337), while all vehicle PBS-treated mice died by day 313 (0/6). Red arrows identify the start (day 168) and the end (day 252) of the treatment period (n=6 mice/group); *$p < 0.05$; ****$p < 0.0001$, compared with vehicle PBS-treated mice; long-rank test.

Supplementary Figure S4.- Comparative LN pathology determination in lupus-prone NZBW F1 mice after administration of both C4BP isoforms: C4BP(β+) and C4BP(β-). (a) Schematic administration schedule and dosage for intraperitoneal (*ip*) injection of C4BP(β+), C4BP(β-) and vehicle (PBS) (blue arrows) in NZBW F1 mice. (**b**) Proteinuria was monitored monthly over the course of the assay from week 21 until week 35. Total 24-h urinary protein was determined by Pyrogallol Red-molybdate protein dye-binding assay. Data are normalized by

For Peer Review Only

mouse weight and expressed as cumulative mean values (n= 8 mice/group); *$p < 0.05$ compared with C4BP(β+)-treated and control, PBS-treated mice. **(c)** Blood urea nitrogen (BUN) levels were assessed by a coupled enzyme reaction both before (week 21) and during (weeks 29 and 33) C4BP treatment. Data are expressed as mean ± SD (n= 4 mice/group); *$p < 0.05$; **$p < 0.01$, compared with C4BP(β+)-treated mice (w33). **(d)** Serum levels of anti-dsDNA antibodies correlating with disease activity were measured by ELISA 1 week and 5 weeks after the start of the treatment (weeks 25 and 29). Data are expressed as mean ± SD (n= 3 mice/group); *$p < 0.05$ compared with C4BP(β+)-treated mice (w25); *$p < 0.05$ compared with vehicle PBS-treated mice (w29). (**e**) Kaplan-Meier survival curves from lupus-prone NZBW F1 mice. Cumulative survival curves showed 100% survival (8/8) in the C4BP(β-)-treated mice, 75% survival (6/8) in PBS-treated mice, and 62.5% survival (5/8) in PBS-treated mice at the end of the study (day 252). Red arrows identify the start (day 168) and the end (day 252) of the treatment period (n= 8 mice/group; *$p = 0.06$), compared with C4BP(β+)-treated mice; long-rank test. **(f)** Representative sections of renal cortex from 36-week old mice treated with C4BP(β+) (left), C4BP(β-) (center) and vehicle PBS (right) mice stained with hematoxylin and eosin. Images are shown at 200 μm magnification. The data obtained were used to semi-quantitatively grade histopathology traits indicating active LN (mesangial expansion, endocapillary proliferation, glomerular deposits, extracapillary proliferation and interstitial infiltrates), as well as chronic lesions (tubular atrophy and interstitial fibrosis) (n= 3 mice/group).

Supplementary Figure S5.- Effect of C4BP(β+) and C4BP(β-) treatment in the activity of the classical pathway of complement from NZBW F1 mouse sera. The activity of the classical pathway of complement was measured as deposition of C3b on antibody-opsonized K562 cells and incubated with mouse sera for 30 min at 37 ºC. Deposited C3b was detected using a FITC-labelled antibody and flow cytometry. MFI, median fluorescence intensity.

For Peer Review Only

Complement activity levels of NZW F1 mice analyzed before the start of C4BP treatment (week 21; n= 6 mice/group) and throughout the treatment (weeks 25 (n= 6 mice/group), 29 and 33 (n= 3 mice/group)). Data are expressed as mean ± SD. *$p < 0.05$ compared with both C4BP(β+)-treated and PBS-treated mice. Serum from C57BL6 mice (14-week old; n= 4) was included as a reference control for normal complement activity. Negative controls (Inact.) from all analyzed samples were determined after serum inactivation at 56 ºC for 30 min.

Supplementary Figure S6.- Electrophoretic analysis of plasma-purified human C4BP(β+) and C4BP(β-) isoforms. Both plasma-purified human C4BP(β+) and C4BP(β-) underwent 3-8% gradient SDS-PAGE under non-reducing (NR) and reducing (R) conditions. Under NR conditions, C4BP(β-) is an homooligomer composed of 7 identical α-chains, and C4BP(β+) is an heterooligomer composed of 7 identical α-chains and a unique β-chain. All chains are covalently linked by their C-termini forming a spider-like structure in both isoforms, which migrate as a 500-570 kDa band (upper arrow). The β-chain is always in complex with the vitamin K-dependent anticoagulant PS (70 kDa). Thus, under reducing conditions, the diffuse 70 kDa band (lower arrow) corresponds to the disassembled α-chains in the case of the C4BP(β-) isoform, and to the disassembled PS plus the α-chains in the case of the C4BP(β+) isoform. MW marker: molecular weight marker.

For Peer Review Only

Luque et al. (September 2019) KI-12-18-1865

SUPPLEMENTARY METHODS

Proteins and drugs

C4BP(β-) purification from human plasma (40 liters) involved $BaCl_2$ precipitation followed by four sequential chromatography steps including heparin chromatography, hydrophobic interaction (butyl) chromatography, anion exchange (Q Sepharose) chromatography and, finally, size exclusion (Superdex) chromatography. Analogously, Recombinant C4BP(β-) (rC4BP(β-)) was transiently produced in HEK293cells (Expi293 cells) and purified from the cell culture supernatants through an hydrophobic interaction (butyl) chromatography followed by an anion exchange (Q Sepharose) chromatography, according to Bioingenium protocols (Bioingenium, Barcelona, Spain). All C4BP isoforms (plasma-purified C4BP(β+) and C4BP(β-), and rC4BP(β-)) were concentrated, dialyzed and recovered in PBS buffer, pH 7.4. The purity of C4BP glycoproteins was higher than 85%, as assessed by Tris-Acetate 3-8% SDS-PAGE (NuPAGE precast protein gels; ThermoFisher, Waltham, MA, USA) from 6 μg protein/lane, and further Coomassie Blue staining (**Supplementary Figure S6**, and data not shown). All C4BP proteins employed in the studies were endotoxin-free, as assessed through the Limulus amebocyte lysate test (GenScript, Piscataway, NJ, USA).

CYP (Genoxal®, Baxter Oncology GmbH, Halle/Westfallen, Germany), was resuspended in saline and administered at a dose of 2.5 mg in a final volume of 0.13 ml.

Bone marrow-derived DC (BMDC) generation

Femurs and tibiae of female, 14 weeks-old BALB/c mice (Charles River Laboratories, Wilmington, MA, USA) were removed and purified from the surrounding muscle tissue by

For Peer Review Only

rubbing with sterile tissues and placed in RPMI-1640 medium (Gibco, ThermoFisher). Thereafter intact bones were soaked in 70% ethanol for desinfection. Both ends were cut with scissors and the marrow was flushed with RPMI-1640 medium, using a 1-ml insulin syringe with a 25G needle, onto a cell strainer (BD Biosciences, Bedford, MA, USA) to obtain a uniform single-cell suspension. $1x10^6$ viable bone marrow cells were resuspended in RPMI 1640 supplemented with 100 mg/ml streptomycin, 100 IU/ml penicillin, 2 mM L-glutamine (all from ThermoFischer) and 10% heat-inactivated FBS (Cultek, Madrid Spain) and plated in 60-mm culture plates at 37ºC under 5% CO_2. For surface phenotype determination, BMDCs were generated supplementing cultures with rmGM-CSF (20ng/ml) (Peprotech, London, UK) at days 0, 3 and 6 of culture. C4BP (β-) was added at 5 μg/ml at days 0 and 3 of culture. At day 6, non-adherent cells were re-seeded into 24-well plates with fresh medium at $5x10^5$ cells/ml and were further stimulated for 24h with 10 μg/ml Gardiquimod (InvivoGen, San Diego, CA, USA).

Mice, study design and follow up

Both NZBW F1 and MRL-*lpr* mouse strains (Jackson Laboratory, Bar Harbor, ME, USA) develop spontaneously an autoimmune disease resembling human SLE. The animals were maintained under standard laboratory conditions, at 20-24 ºC and 40-70% relative humidity, with 12-hour fluorescent light/12-hour dark cycle. They were feed standard diet and tap water ad libitium.

The selection of the highest C4BP(β-) dose for *in vivo* administration was based in previous studies employing complement-related proteins in murine models of immune-inflammatory pathologies.[S1–S3] We opted for the beginning of C4BP(β-) and C4BP(β+) treatments at 24 weeks because it has been reported that when 23 weeks old, while histologically normal, NZBW F1 mice already show faint staining of the glomeruli with anti-IgG and increased expression of several inflammatory markers.[S4] Analogously, at the beginning of C4BP(β-)

For Peer Review Only

administration, 10 week old MRL-*lpr* mice were fully hypocomplementemic (data not shown), indicative of high levels of circulating ICs and active disease.[S5]

Neither toxicity nor behavioral changes were observed in the mice as a consequence of C4BP(β-), C4BP(β+) or CYP administration. Body weight was determined twice monthly (NZBW F1 mice) or weekly (MRL-*lpr* mice) from the beginning to the end of follow-up. Mice were placed in metabolic cages to collect 24 h urine specimens before the onset of treatment and monthly (NZBW F1 mice) or biweekly (MRL-*lpr* mice) thereafter. Blood was obtained from the tail vein at monthly intervals and at the sacrifice. Kidneys were dissected and processed for histological, biochemical and molecular analyses at the end of the study.

In MRL-*lpr* mice, macroscopic SLE-like skin lesions from the interscapular region, the snout and the ears were scored weekly in a semiquantitative manner using a 0 to 4 scoring system: 0, no visible skin changes; 1, minimal hair loss with redness and a few scattered lesions; 2, redness and hair loss with a small area of involvement (< 0,5 cm^2); 3, redness, scabbing, and lesion(s) with total area > 0.5, but < 1.0 cm^2; and 4, redness, scabbing, and lesion(s) with total area > 1.0 cm^2.

All experiments were carried out in accordance with current EU legislation on animal experimentation and were approved by ‘‘CEEA: Animal Experimentation Ethics Committee”, the Institutional Ethics University of Barcelona Committee for Animal Research, and the Generalitat de Catalunya (DARP: 8765).

ELISA for anti-human C4BP(β-) detection

To assess the development of antibodies against administered human rC4BP(β-) by the NZBW F1 mice, we set up an indirect ELISA assay. Briefly, we immobilized C4BP(β-) (200 ng/100 µl/well, dissolved in coating buffer: 100 mM Na_2CO_3 / $NaHCO_3$, pH 9.6) by direct adsorption in a 96-well plate overnight at 4 ºC. Next, the plate was blocked with Tris-Tween (50

For Peer Review Only

mM Tris pH 7.4 + 150 mM NaCl + 0.2% Tween 20) + 1% BSA (100 ml/well) for 1h at room temp. The collected mouse sera were diluted to 1:500 in Tris-Tween + 1% BSA and incubated in duplicate to the plate (100 µl/well) for 1.5 h at room temp. Human C4BP(β-)-specific antibodies were detected by incubation with an anti-mouse IgG horseradish peroxidase (HRP)-conjugated secondary antibody (Agilent Technologies, Santa Clara, CA, USA) (1:10,000 dilution) in Tris-Tween + 1% BSA for 30 min. at room temp. Washing between steps was performed with Tris-Tween. Finally, the plate was developed with TMB (3,3',5,5'-tetramethylbenzidine) HRP substrate, stopped with sulfuric acid (1N H_2SO_4) and the absorbances were read at 450 nm in a microtiter plate reader. Negative controls included sera from CYP- and PBS-treated mice.

Flow cytometry

Cell surface phenotypes were analyzed using FITC-conjugated anti–CD80 (16-10A1) and PE-conjugated anti-CD86 (PO3.3) mAbs (all from Miltenyi Biotec, Bergisch Gladbach, Germany). After washing with PBS, cells were subsequently stained with 3µl mAbs/10^5 cells in 100 µl FACS buffer (PBS containing 1% BSA and 0.1% sodium azide) for 15 min at room temperature. To exclude debris, BMDCs were gated according to forward scatter (FSC) and side scatter (SSC) parameters. Staining with 7-aminoactinomycin D (ThermoFischer) was also employed to assess the viability status of BMDCs. Stained cells were analyzed using a FACSCanto II flow cytometer equipped with FACSDiva software (Becton Dickinson, Franklin Lakes, NJ, USA). Subsequent analyses were performed through FlowJo software (Flowjo LLC, Ashland, OR, USA).

Renal histopathology

For Peer Review Only

To determine the extent of renal damage, all sections were analyzed by two blinded pathologists. Typical glomerular active lesions of LN were evaluated: mesangial expansion, endocapillary proliferation, glomerular deposits, extracapillary proliferation and interstitial infiltrates, as well as tubulointerstitial chronic lesions: tubular atrophy and interstitial fibrosis. Lesions were graded semi-quantitatively using a four-point scoring system: (-) null, (+) low, (++) moderate, (+++) severe. Glomerular cross-sectional area (μm^2) was calculated based on average area of 150 glomeruli in each group, from digitized images taken at x100 (3 mice/group), measured using ImageJ v1.52c software (http://fiji.sc/; NIH, Bethesda, MD, USA).

Immunofluorescent determination of renal IC and complement deposition

Kidney slices were fixed in 4% paraformaldehyde, embedded in Tissue Tec OCT compound (Sakura, Alpen aan den Rijn, Netherlands) and stored at -80 ºC. Five-µm cryostat sections were used for confocal microscopy to quantify the mean fluorescence intensity of the Cy5.5 fluorochrome. At least 10 glomeruli per section were visualized and photographed with an immunofluorescence confocal microscope Leica TCS-SL spectral (Leica Microsystems GmbH, Wetzlar, Germany). Fluorescence was quantified with Leica software and expressed as mean fluorescence intensity (MFI).

Complement activity assay

The activity of the classical pathway of complement was determined by C3b deposition on K562 cells (ATCC, LGC Standards, Barcelona, Spain) opsonized with rabbit polyclonal antibodies (Agrisera, Vännäs, Sweden). Briefly, K562 cells were cultured in suspension in Dulbecco modified Eagle medium (DMEM) supplemented with 10% heat-inactivated FBS, 100

For Peer Review Only

mg/ml streptomycin, 100 IU/ml penicillin, 2 mM L-glutamine (all from ThermoFischer). The cells were washed twice in cold PBS, and 10^6 cells were added to reaction tubes containing PBS with 2 mM $MgCl_2$, 0.15 mM $CaCl_2$, 5 mg/ml of opsonizing antibodies and 10% mouse sera in a total volume of 100 µl. After 30 min incubation at 37ºC, cells were washed with cold FACS buffer. The amount of deposited C3b was measured using FITC-conjugated goat IgG fraction to mouse complement C3 antibody (MP Biomedicals, Solon, OH, USA) diluted 1:100, and allowed to bind for 1 h at 4ºC. The cells were washed three times, resuspended with cold FACS buffer, and analyzed in a FACSCanto II flow cytometer equipped with FACSDiva software (Becton Dickinson).

Immunohistochemistry

Paraffin-processed sections (5 µm) were deparaffinized in xylene, rehydrated in graded ethanol solutions, rinsed in distilled water and treated with 3% hydrogen peroxide in methanol (30 min at room temp. (RT)) to remove endogenous peroxidase activity. The sections were further incubated 30 min at RT with blocking solution (5% goat serum, 0.1% Tween 20 in PBS, pH 7.2), and incubated overnight at 4ºC with the primary antibodies, washed in PBS and incubated with the appropriate secondary antibodies for 30-60 min at RT. Colour was developed using 3,3'-diaminobenzidine (DAB) and sections were counterstained with hematoxylin before dehydration, clearing, and mounting. Negative controls in which the primary antibody was replaced with PBS were used to test for non-specific binding (data not shown).

TUNEL Assay

Briefly, 5 µm thick deparaffinized sections were pretreated with proteinase K for 30 min at RT. After washing in deionized water, the endogenous peroxidase was inactivated using 3%

For Peer Review Only

H_2O_2 in methanol for 5 min, followed by incubation with TdT enzyme at 37°C for 1 h. Next, sections were immersed in TdT Stop buffer and incubated with Streptavidin-HRP solution at 37 ºC for 10 min followed by DAB solution. Slices were counterstained with 1% methyl green. TUNEL-positive cells were assessed by light microscopy. The number of cortical apoptotic cells was quantified in 10 fields from 3 section samples/group and given as apoptotic cells/field. Ten glomeruli per section (30 glomeruli/group) were also quantified to establish the number of apoptotic cells per glomerular cut section (cells/*gcs*). ImageJ v1.52c software (NIH) was employed to analyze digitized images at x200 and x400, respectively.

Differential gene expression analysis

Total RNA from mouse kidneys was extracted using the RNeasy Mini Kit (Qiagen, Hilden, Germany). Reverse transcription was performed using the High-capacity cDNA archive kit (Applied BioSystems, Carlsbad, CA, USA). Gene expression profiling was performed in 384-well microfluidic cards pre-loaded with 377 gene expression assays for transcripts relevant in murine LN. [S6-S8] Four wells per card included the 18S gene expression assay as internal control. We used one card for each pool (2-3 mice/pool; 3 cards/group). Data were obtained with SDS v2.4 and RQ Manager v1.2.1, analyzed with DataAssist software v3.0 (all from Applied Biosystems) and normalized using 3 endogenous controls (*Actb, Gapdh* and *Gusb*). The values obtained were relativized using the vehicle PBS-treated group as reference.

Differentially expressed genes were analyzed using the Ingenuity Pathway Analysis (IPA) (Ingenuity Systems, Qiagen) to identify biological and molecular networks differentially regulated in the LN model. IPA core analysis is a source of gene-interaction based pathway analysis including canonical pathways and a knowledge database based on scientific findings. Differentially expressed genes at least 1.8-fold upregulated or downregulated were imported and analyzed in the IPA database. Based on the direct or indirect connectivity of genes as disclosed

For Peer Review Only

in the literature, genes were mapped onto biological pathways and disease networks. A *P* value of < 0.05 (Fisher exact test) was used as the cutoff for significant biological functions, networks, and pathways, and they were ranked by ratio. Downstream effects analysis was undertaken to identify key biological processes influenced by differentially expressed genes. Statistical significance of the overlap between two groups of genes from our dataset and from the "Ingenuity® Knowledge Base" was given as overlap p-value, and significant process or pathway directionality was predicted when 2 < Z-score < -2.

Selected gene transcripts were further validated in individual mouse kidney samples by RT-qPCR using the corresponding inventoried TaqMan Gene Expression Assays (Applied BioSystems). Quantification was achieved through the ΔΔCt method. A relative fold change in mRNA abundance was calculated with the equation $2^{-\Delta\Delta Ct}$, employing *Gusb* as endogenous reference transcript.

Pathway annotation of the RT-qPCR-validated gene set was performed through PathwAX, which uses the comprehensive network FunCoup to analyze network crosstalk between a query gene list and KEGG pathways.

Mouse cytokine array

Serum was obtained by centrifugation of blood samples at sacrifice (1500 g, 10 min, 4ºC). Tissue lysates were obtained by kidney homogenization in PBS supplemented with the protease inhibitors aprotinin (Sigma-Aldrich), leupeptin and pepstatin (both from Tocris Bioscience, Bristol, UK) (all 10µg/ml) using a Dounce Homogenizer (Knotes Glass, Vineland, NJ, USA). Triton X-100 was added to a final concentration of 1% before the lysates underwent freezing at -80°C. After thawing, the lysates were centrifuged at 10000 g for 5 min. Pooled samples (100 µl serum, or 300 µg protein extracts; 2 mice/group) were analyzed using the Proteome Profiler Array "Mouse Cytokine Array Panel A" kit (R&D Systems), according to the

For Peer Review Only

manufacturer's instructions, to determine the relative levels of 40 cytokines and chemokines and acute phase proteins.

For Peer Review Only

References

S1. Blom AM, Nandakumar KS, Holmdahl R. C4b-binding protein (C4BP) inhibits development of experimental arthritis in mice. *Ann Rheum Dis*. 2009;68:136-142.

S2. Rodriguez W, Mold C, Marnell LL, et al. Prevention and reversal of nephritis in MRL/lpr mice with a single injection of C-reactive protein. *Arthritis Rheum*. 2006;54:325-335.

S3. Fakhouri F, de Jorge EG, Brune F, et al. Treatment with human complement factor H rapidly reverses renal complement deposition in factor H-deficient mice. *Kidney Int*. 2010;78:279-286.

S4. Schiffer L, Bethunaickan R, Ramanujam M, et al. Activated renal macrophages are markers of disease onset and disease remission in lupus nephritis. *J Immunol*. 2008;180:1938-1947.

S5 Andrews BS, Eisenberg RA, Theofilopoulos AN, et al. Spontaneous murine lupus-like syndromes. Clinical and immunopathological manifestations in several strains. *J Exp Med.* 1978; 148:1198-1215.

S6. Berthier CC, Bethunaickan R, Gonzalez-Rivera T, et al. Cross-species transcriptional network analysis defines shared inflammatory responses in murine and human lupus nephritis. *J Immunol.* 2012;189:988-1001.

S7. Bethunaickan R, Berthier CC, Zhang W, et al. Comparative transcriptional profiling of 3 murine models of SLE nephritis reveals both unique and shared regulatory networks. *PLoS ONE* 2013;8:e77489.

S8. Bethunaickan R, Berthier CC, Zhang W, et al. Identification of stage-specific genes associated with lupus nephritis and response to remission induction in (NZB x NZW)F1 and NZM2410 mice. *Arthritis Rheum*. 2014;66:2246-2258

For Peer Review Only

Table S1.- List of relevant SLE genes included in the customized *TaqMan* Low Density Array.

Gene Symbol	Assay ID	UniGene ID	Gene name
Acad8	Mm00482266_m1	Mm.289244	acyl-Coenzyme A dehydrogenase family, member 8
Ace	Mm00802048_m1	Mm.754	angiotensin I converting enzyme (peptidyl-dipeptidase A) 1
Acsl1	Mm00484217_m1	Mm.210323	acyl-CoA synthetase long-chain family member 1
Acsl3	Mm01255804_m1	Mm.276016	acyl-CoA synthetase long-chain family member 3
Actr3	Mm02342769_g1	Mm.183102	ARP3 actin-related protein 3
Ada	Mm00545720_m1	Mm.388	adenosine deaminase
Adh1	Mm00507711_m1	Mm.2409	alcohol dehydrogenase 1 (class I)
Adh7	Mm00507750_m1	Mm.8473	alcohol dehydrogenase 7 (class IV), mu or sigma polypeptide
Adhfe1	Mm00613830_m1	Mm.28514	alcohol dehydrogenase, iron containing, 1
Adsl	Mm00507759_m1	Mm.38151	adenylosuccinate lyase
Agt	Mm00599662_m1	Mm.301626	angiotensinogen (serpin peptidase inhibitor, clade A, member 8)
Ahcyl1	Mm00461101_m1	Mm.220328	S-adenosylhomocysteine hydrolase-like 1
Ahcyl2	Mm00619649_m1	Mm.210899	S-adenosylhomocysteine hydrolase-like 2
Aifm1	Mm00442540_m1	Mm.240434	apoptosis-inducing factor, mitochondrion-associated 1
Aim2	Mm01295719_m1	Mm.131453	absent in melanoma 2
Akr1a1	Mm00480608_m1	Mm.30085	aldo-keto reductase family 1, member A1 (aldehyde reductase)
Aldh2	Mm00477463_m1	Mm.284446	aldehyde dehydrogenase 2, mitochondrial
Aldh3a2	Mm00839320_m1	Mm.398221	aldehyde dehydrogenase family 3, subfamily A2
Aldh3b1	Mm00550698_m1	Mm.109341	aldehyde dehydrogenase 3 family, member B1
Aldh4a1	Mm00615268_m1	Mm.273571	aldehyde dehydrogenase 4 family, member A1
Aldh6a1	Mm00506227_m1	Mm.247510	aldehyde dehydrogenase family 6, subfamily A1
Aldh7a1	Mm00519645_m1	Mm.30250	aldehyde dehydrogenase family 7, member A1
Aldh9a1	Mm00480240_m1	Mm.292539	aldehyde dehydrogenase 9, subfamily A1
Apoc3	Mm00445670_m1	Mm.390161	apolipoprotein C-III
Apoe	Mm01307193_g1	Mm.305152	apolipoprotein E
Arf6	Mm00500208_s1	Mm.27308	ADP-ribosylation factor 6
Arg1	Mm00475988_m1	Mm.154144	arginase, liver
Arg2	Mm00477592_m1	Mm.3506	arginase type II
Arpc1b	Mm00834862_m1	Mm.30010	actin related protein 2/3 complex, subunit 1B
Arpc2	Mm01254383_m1	Mm.337038	actin related protein 2/3 complex, subunit 2
Arpc3	Mm01199871_m1	Mm.275942	actin related protein 2/3 complex, subunit 3
Arpc5	Mm04208715_m1	Mm.288974	actin related protein 2/3 complex, subunit 5
Atf4	Mm00515325_g1	Mm.641	activating transcription factor 4
Atp5b	Mm00443967_g1	Mm.238973	ATP synthase, H+ transporting mitochondrial F1 complex, beta subunit
Atp5f1	Mm01296543_g1	Mm.251152	ATP synthase, H+ transporting, mitochondrial F0 complex, subunit B1
Atp5g3	Mm01334541_g1	Mm.2966	ATP synthase, H+ transporting, mitochondrial F0 complex, subunit C3 (subunit 9)
Auh	Mm00479363_m1	Mm.252034	AU RNA binding protein/enoyl-coenzyme A hydratase
B2m	Mm00437762_m1	Mm.163	beta-2 microglobulin
Batf3	Mm01318274_m1	Mm.6922	basic leucine zipper transcription factor, ATF-like 3
Bckdha	Mm00476112_m1	Mm.25848	branched chain ketoacid dehydrogenase E1, alpha polypeptide
Bckdhb	Mm01177077_m1	Mm.12819	branched chain ketoacid dehydrogenase E1, beta polypeptide

For Peer Review Only

Blk	Mm00432077_m1	Mm.3962	B lymphoid kinase
Btk	Mm00442712_m1	Mm.4475	Bruton agammaglobulinemia tyrosine kinase
C1qa	Mm00432142_m1	Mm.439957	complement component 1, q subcomponent, alpha polypeptide
C1qb	Mm01179619_m1	Mm.2570	complement component 1, q subcomponent, beta polypeptide
C1qc	Mm00776126_m1	Mm.439732	complement component 1, q subcomponent, C chain
C1ra	Mm04206253_g1	Mm.333375	complement component 1, r subcomponent A
C1s1	Mm00663210_mH	Mm.219527	complement component 1, s subcomponent 1
C3	Mm00437838_m1	Mm.19131	complement component 3
C3ar1	Mm02620006_s1	Mm.2408	complement component 3a receptor 1
C4bp	Mm00432150_m1	Mm.306720	complement component 4 binding protein
C6	Mm00489521_m1	Mm.20247	complement component 6
C8a	Mm00521627_m1	Mm.197638	complement component 8, alpha polypeptide
C9	Mm00442739_m1	Mm.29095	complement component 9
Casp1	Mm00438023_m1	Mm.1051	caspase 1
Casp3	Mm01195085_m1	Mm.34405	caspase 3
Cat	Mm00437992_m1	Mm.4215	catalase
Cbs	Mm00460654_m1	Mm.206417	cystathionine beta-synthase
Ccl2	Mm00441242_m1	Mm.290320	chemokine (C-C motif) ligand 2
Ccl5	Mm01302427_m1	Mm.284248	chemokine (C-C motif) ligand 5
Ccl9	Mm00441260_m1	Mm.416125	chemokine (C-C motif) ligand 9
Ccr1	Mm00438260_s1	Mm.274927	chemokine (C-C motif) receptor 1
Ccr2	Mm00438270_m1	Mm.6272	chemokine (C-C motif) receptor 2
Ccr5	Mm01963251_s1	Mm.14302	chemokine (C-C motif) receptor 5
Ccr6	Mm99999114_s1	Mm.8007	chemokine (C-C motif) receptor 6
Ccr7	Mm01301785_m1	Mm.2932	chemokine (C-C motif) receptor 7
Ccs	Mm00444148_m1	Mm.434411	copper chaperone for superoxide dismutase
Cd14	Mm00438094_g1	Mm.3460	CD14 antigen
Cd19	Mm00515420_m1	Mm.4360	CD19 antigen
Cd1d1	Mm00783541_s1	Mm.1894	CD1d1 antigen
Cd207	Mm00523545_m1	Mm.136079	CD207 antigen
Cd22	Mm00515432_m1	Mm.260994	CD22 antigen
Cd274	Mm00452054_m1	Mm.245363	CD274 antigen
Cd276	Mm00506020_m1	Mm.5356	CD276 antigen
Cd28	Mm00483137_m1	Mm.255003	CD28 antigen
Cd300lb	Mm01701741_m1	Mm.185355	CD300 antigen like family member B
Cd3d	Mm00442746_m1	Mm.4527	CD3 antigen, delta polypeptide
Cd3g	Mm00438095_m1	Mm.335106	CD3 antigen, gamma polypeptide
Cd40	Mm00441891_m1	Mm.271833	CD40 antigen
Cd40lg	Mm00441911_m1	Mm.4861	CD40 ligand
Cd48	Mm00455932_m1	Mm.1738	CD48 antigen
Cd5	Mm00432417_m1	Mm.779	CD5 antigen
Cd74	Mm00658576_m1	Mm.439737	CD74 antigen (invariant polypeptide of major histocompatibility complex, class II antigen-associated)
Cd79b	Mm00434143_m1	Mm.2987	CD79B antigen
Cd80	Mm00711660_m1	Mm.89474	CD80 antigen
Cd83	Mm00486868_m1	Mm.57175	CD83 antigen
Cd86	Mm00444543_m1	Mm.1452	CD86 antigen

For Peer Review Only

Cdt1	Mm00466006_m1	Mm.21873	chromatin licensing and DNA replication factor 1
Cebpb	Mm00843434_s1	Mm.439656	CCAAT/enhancer binding protein (C/EBP), beta
Cfb	Mm00433918_g1	Mm.653	complement factor B
Cfh	Mm01299248_m1	Mm.8655	complement component factor h
Cfi	Mm00432470_m1	Mm.117180	complement component factor i
Chek2	Mm00443839_m1	Mm.279308	checkpoint kinase 2
Chga	Mm00514341_m1	Mm.4137	chromogranin A
Cldn1	Mm00516701_m1	Mm.289441	claudin 1
Cldn7	Mm00516817_m1	Mm.281896	claudin 7
Clec10a	Mm00546125_g1	Mm.252405	C-type lectin domain family 10, member A
Clec4n	Mm00490934_m1	Mm.271782	C-type lectin domain family 4, member n
Clec7a	Mm01183349_m1	Mm.239516	C-type lectin domain family 7, member a
Clu	Mm01197002_m1	Mm.200608	clusterin
Col18a1	Mm00487131_m1	Mm.4352	collagen, type XVIII, alpha 1
Col1a1	Mm00801666_g1	Mm.277735	collagen, type I, alpha 1
Col1a2	Mm00483888_m1	Mm.277792	collagen, type I, alpha 2
Col3a1	Mm01254476_m1	Mm.249555	collagen, type III, alpha 1
Col4a1	Mm01210125_m1	Mm.738	collagen, type IV, alpha 1
Cox11	Mm01615963_g1	Mm.151940	cytochrome c oxidase assembly protein 11
Cox15	Mm00523096_m1	Mm.248237	cytochrome c oxidase assembly protein 15
Cox5a	Mm01176957_g1	Mm.273403	cytochrome c oxidase subunit Va
Cox5b	Mm00833840_g1	Mm.180182	cytochrome c oxidase subunit Vb
Cox6a1	Mm01612194_m1	Mm.43415	cytochrome c oxidase subunit VIa polypeptide 1
Cox6b1	Mm00824357_m1	Mm.400	cytochrome c oxidase, subunit VIb polypeptide 1
Cox8a	Mm02342396_g1	Mm.14022	cytochrome c oxidase subunit VIIIa
Cpeb1	Mm01314928_m1	Mm.273122	cytoplasmic polyadenylation element binding protein 1
Csf1	Mm00432686_m1	Mm.795	colony stimulating factor 1 (macrophage)
Csf1r	Mm01266652_m1	Mm.22574	colony stimulating factor 1 receptor
Csf2rb	Mm00655745_m1	Mm.235324	colony stimulating factor 2 receptor, beta, low-affinity (granulocyte-macrophage)
Cst7	Mm00438349_m1	Mm.12965	cystatin F (leukocystatin)
Ctgf	Mm01192932_g1	Mm.390287	connective tissue growth factor
Ctla4	Mm00486849_m1	Mm.390	cytotoxic T-lymphocyte-associated protein 4
Ctss	Mm01255859_m1	Mm.3619	cathepsin S
Cx3cl1	Mm00436454_m1	Mm.103711	chemokine (C-X3-C motif) ligand 1
Cx3cr1	Mm02620111_s1	Mm.44065	chemokine (C-X3-C motif) receptor 1
Cxcl1	Mm04207460_m1	Mm.21013	chemokine (C-X-C motif) ligand 1
Cxcl10	Mm00445235_m1	Mm.877	chemokine (C-X-C motif) ligand 10
Cxcl11	Mm00444662_m1	Mm.131723	chemokine (C-X-C motif) ligand 11
Cxcl13	Mm04214185_s1	Mm.10116	chemokine (C-X-C motif) ligand 13
Cxcl16	Mm00469712_m1	Mm.425692	chemokine (C-X-C motif) ligand 16
Cxcl2	Mm00436450_m1	Mm.4979	chemokine (C-X-C motif) ligand 2
Cxcl9	Mm00434946_m1	Mm.766	chemokine (C-X-C motif) ligand 9
Cxcr4	Mm01996749_s1	Mm.1401	chemokine (C-X-C motif) receptor 4
Cxcr6	Mm02620517_s1	Mm.124289	chemokine (C-X-C motif) receptor 6
Cyc1	Mm00470540_m1	Mm.29196	cytochrome c-1
Dbf4	Mm01324087_m1	Mm.292470	DBF4 homolog (S. cerevisiae)

For Peer Review Only

Ddr1	Mm01273496_m1	Mm.5021	discoidin domain receptor family, member 1
Dhrs4	Mm00472717_m1	Mm.27427	dehydrogenase/reductase (SDR family) member 4
Dld	Mm00432831_m1	Mm.3131	dihydrolipoamide dehydrogenase
Dnaja1	Mm00787254_s1	Mm.27897	DnaJ (Hsp40) homolog, subfamily A, member 1
Egln3	Mm00472200_m1	Mm.133037	egl-9 family hypoxia-inducible factor 3
Eng	Mm00468256_m1	Mm.225297	endoglin
Ep300	Mm00625535_m1	Mm.258397	E1A binding protein p300
Epas1	Mm01236112_m1	Mm.1415	endothelial PAS domain protein 1
Ephx2	Mm01313813_m1	Mm.15295	epoxide hydrolase 2, cytoplasmic
Ereg	Mm00514794_m1	Mm.4791	epiregulin
F3	Mm00438853_m1	Mm.273188	coagulation factor III
Fasl	Mm00438864_m1	Mm.3355	Fas ligand (TNF superfamily, member 6)
Fcer1g	Mm02343757_m1	Mm.22673	Fc receptor, IgE, high affinity I, gamma polypeptide
Fcgr1	Mm00438874_m1	Mm.150	Fc receptor, IgG, high affinity I
Fcgr3	Mm00438882_m1	Mm.22119	Fc receptor, IgG, low affinity III
Fcgr4	Mm00519988_m1	Mm.251254	Fc receptor, IgG, low affinity IV
Fga	Mm00802584_m1	Mm.88793	fibrinogen alpha chain
Fgb	Mm00805336_m1	Mm.30063	fibrinogen beta chain
Fgg	Mm00513575_m1	Mm.16422	fibrinogen gamma chain
Fli1	Mm00484410_m1	Mm.258908	Friend leukemia integration 1
Fmo1	Mm00515795_m1	Mm.976	flavin containing monooxygenase 1
Fmo2	Mm00490159_m1	Mm.10929	flavin containing monooxygenase 2
Fmo4	Mm00467393_m1	Mm.155164	flavin containing monooxygenase 4
Fn1	Mm01256744_m1	Mm.193099	fibronectin 1
Fos	Mm00487425_m1	Mm.246513	FBJ osteosarcoma oncogene
Foxp3	Mm00475162_m1	Mm.182291	forkhead box P3
Fyn	Mm00433373_m1	Mm.4848	Fyn proto-oncogene
Got1	Mm01195792_g1	Mm.19039	glutamic-oxaloacetic transaminase 1, soluble
Gpnmb	Mm01328587_m1	Mm.302602	glycoprotein (transmembrane) nmb
Gss	Mm00515065_m1	Mm.252316	glutathione synthetase
Gsto1	Mm00599866_m1	Mm.378931	glutathione S-transferase omega 1
Havcr1	Mm00506686_m1	Mm.17771	hepatitis A virus cellular receptor 1
Hck	Mm01241463_m1	Mm.715	hemopoietic cell kinase
Hmox1	Mm00516005_m1	Mm.276389	heme oxygenase 1
Hnf4a	Mm01247712_m1	Mm.202383	hepatic nuclear factor 4, alpha
Hspe1	Mm00434083_m1	Mm.215667	heat shock protein 1 (chaperonin 10)
Icam1	Mm00516023_m1	Mm.435508	intercellular adhesion molecule 1
Icos	Mm00497600_m1	Mm.42044	inducible T cell co-stimulator
Id1	Mm00775963_g1	Mm.444	inhibitor of DNA binding 1
Idh1	Mm00516030_m1	Mm.9925	isocitrate dehydrogenase 1 (NADP+), soluble
Idh3a	Mm00499674_m1	Mm.279195	isocitrate dehydrogenase 3 (NAD+) alpha
Idh3b	Mm00504589_m1	Mm.29590	isocitrate dehydrogenase 3 (NAD+) beta
Idh3g	Mm00599686_g1	Mm.14825	isocitrate dehydrogenase 3 (NAD+), gamma
Ifi202b	Mm00839397_m1	Mm.218770	interferon activated gene 202B
Ifi44	Mm00505670_m1	Mm.30756	interferon-induced protein 44
Ifih1	Mm00459183_m1	Mm.136224	interferon induced with helicase C domain 1

For Peer Review Only

Ifng	Mm01168134_m1	Mm.240327	interferon gamma
Igfbp1	Mm00515154_m1	Mm.21300	insulin-like growth factor binding protein 1
Igfbp6	Mm00599696_m1	Mm.358609	insulin-like growth factor binding protein 6
Ikbke	Mm00444862_m1	Mm.386783	inhibitor of kappaB kinase epsilon
Ikzf1	Mm01187882_m1	Mm.103545	IKAROS family zinc finger 1
Il10	Mm00439614_m1	Mm.874	interleukin 10
Il10ra	Mm00434151_m1	Mm.379327	interleukin 10 receptor, alpha
Il12a	Mm00434165_m1	Mm.103783	interleukin 12a
Il12b	Mm00434174_m1	Mm.239707	interleukin 12b
Il17a	Mm00439618_m1	Mm.5419	interleukin 17A
Il18	Mm00434225_m1	Mm.1410	interleukin 18
Il1b	Mm00434228_m1	Mm.222830	interleukin 1 beta
Il1f6	Mm00457645_m1	Mm.133095	interleukin 1 family, member 6
Il1r2	Mm00439629_m1	Mm.1349	interleukin 1 receptor, type II
Il23a	Mm01160011_g1	Mm.125482	interleukin 23, alpha subunit p19
Il27	Mm00461162_m1	Mm.222632	interleukin 27
Il27ra	Mm00497259_m1	Mm.38386	interleukin 27 receptor, alpha
Il2rg	Mm00442885_m1	Mm.2923	interleukin 2 receptor, gamma chain
Il33	Mm00505403_m1	Mm.182359	interleukin 33
Il4	Mm00445259_m1	Mm.276360	interleukin 4
Il7r	Mm00434295_m1	Mm.389	interleukin 7 receptor
Inpp5d	Mm00494987_m1	Mm.15105	inositol polyphosphate-5-phosphatase D
Irak1	Mm01193538_m1	Mm.38241	interleukin-1 receptor-associated kinase 1
Irf1	Mm01288580_m1	Mm.105218	interferon regulatory factor 1
Irf4	Mm00516431_m1	Mm.4677	interferon regulatory factor 4
Irf5	Mm00496477_m1	Mm.6479	interferon regulatory factor 5
Irf7	Mm00516793_g1	Mm.3233	interferon regulatory factor 7
Irf8	Mm00492567_m1	Mm.334861	interferon regulatory factor 8
Irf9	Mm00492679_m1	Mm.2032	interferon regulatory factor 9
Itga4	Mm01277951_m1	Mm.31903	integrin alpha 4
Itgam	Mm00434455_m1	Mm.262106	integrin alpha M
Itgb2	Mm00434513_m1	Mm.1137	integrin beta 2
Jak3	Mm00439973_m1	Mm.249645	Janus kinase 3
Jun	Mm00495062_s1	Mm.275071	jun proto-oncogene
Klk11	Mm00480210_g1	Mm.154276	kallikrein related-peptidase 11
Klkb1	Mm00434658_m1	Mm.482691	kallikrein B, plasma 1
Lat	Mm00456761_m1	Mm.10280	linker for activation of T cells
Lck	Mm00802897_m1	Mm.293753	lymphocyte protein tyrosine kinase
Lcp2	Mm01187570_m1	Mm.265350	lymphocyte cytosolic protein 2
Lrrk2	Mm00481934_m1	Mm.37558	leucine-rich repeat kinase 2
Ltb	Mm00434774_g1	Mm.1715	lymphotoxin B
Ly96	Mm01227593_m1	Mm.116844	lymphocyte antigen 96
Lyn	Mm01217488_m1	Mm.317331	Yamaguchi sarcoma viral (v-yes-1) oncogene homolog
Maob	Mm00555412_m1	Mm.241656	monoamine oxidase B
Map3k1	Mm00803707_m1	Mm.15918	mitogen-activated protein kinase kinase kinase 1
Map3k3	Mm00803725_m1	Mm.27041	mitogen-activated protein kinase kinase kinase 3

For Peer Review Only

Map3k8	Mm00432637_m1	Mm.3275	mitogen-activated protein kinase kinase kinase 8
Mapk9	Mm00444239_m1	Mm.68933	mitogen-activated protein kinase 9
Mat2b	Mm00506137_m1	Mm.293771	methionine adenosyltransferase II, beta
Mmp2	Mm00439498_m1	Mm.29564	matrix metallopeptidase 2
Mmp9	Mm00442991_m1	Mm.4406	matrix metallopeptidase 9
Mpo	Mm01298424_m1	Mm.4668	myeloperoxidase
Ms4a1	Mm00545909_m1	Mm.4046	membrane-spanning 4-domains, subfamily A, member 1
Msr1	Mm00446214_m1	Mm.239291	macrophage scavenger receptor 1
Myl9	Mm01251442_m1	Mm.271770	myosin, light polypeptide 9, regulatory
Ncf1	Mm00447921_m1	Mm.425296	neutrophil cytosolic factor 1
Ndrg2	Mm00443481_g1	Mm.26722	N-myc downstream regulated gene 2
Ndufa10	Mm00600325_m1	Mm.248778	NADH dehydrogenase (ubiquinone) 1 alpha subcomplex 10
Ndufa3	Mm01329704_g1	Mm.17851	NADH dehydrogenase (ubiquinone) 1 alpha subcomplex, 3
Ndufa8	Mm00503351_m1	Mm.19834	NADH dehydrogenase (ubiquinone) 1 alpha subcomplex, 8
Ndufa9	Mm00481216_m1	Mm.29939	NADH dehydrogenase (ubiquinone) 1 alpha subcomplex, 9
Ndufaf1	Mm00452828_m1	Mm.5390	NADH dehydrogenase (ubiquinone) 1 alpha subcomplex, assembly factor 1
Ndufb10	Mm01300078_m1	Mm.1129	NADH dehydrogenase (ubiquinone) 1 beta subcomplex, 10
Ndufb2	Mm01157852_m1	Mm.29415	NADH dehydrogenase (ubiquinone) 1 beta subcomplex, 2
Ndufb5	Mm00452592_m1	Mm.28058	NADH dehydrogenase (ubiquinone) 1 beta subcomplex, 5
Ndufb6	Mm01208591_g1	Mm.1103	NADH dehydrogenase (ubiquinone) 1 beta subcomplex, 6
Ndufs1	Mm00523640_m1	Mm.290791	NADH dehydrogenase (ubiquinone) Fe-S protein 1
Ndufs5	Mm02600127_g1	Mm.42805	NADH dehydrogenase (ubiquinone) Fe-S protein 5
Ndufs7	Mm01144210_m1	Mm.28712	NADH dehydrogenase (ubiquinone) Fe-S protein 7
Nfatc3	Mm01249200_m1	Mm.383185	nuclear factor of activated T cells, cytoplasmic, calcineurin dependent 3
Nfkb2	Mm00479810_g1	Mm.102365	nuclear factor of kappa light polypeptide gene enhancer in B cells 2, p49/p100
Nfkbie	Mm01269649_m1	Mm.57043	nuclear factor of kappa light polypeptide gene enhancer in B cells inhibitor, epsilon
Nisch	Mm00452152_m1	Mm.298728	nischarin
Nlrp3	Mm00840904_m1	Mm.54174	NLR family, pyrin domain containing 3
Nox4	Mm00479246_m1	Mm.31748	NADPH oxidase 4
Npy	Mm03048253_m1	Mm.154796	neuropeptide Y
Osmr	Mm01307326_m1	Mm.10760	oncostatin M receptor
Park7	Mm00498538_m1	Mm.277349	Parkinson disease (autosomal recessive, early onset) 7
Pcca	Mm00454899_m1	Mm.23876	propionyl-Coenzyme A carboxylase, alpha polypeptide
Pccb	Mm00452663_m1	Mm.335385	propionyl Coenzyme A carboxylase, beta polypeptide
Pdcd1lg2	Mm00451734_m1	Mm.116737	programmed cell death 1 ligand 2
Pdgfrb	Mm00435546_m1	Mm.4146	platelet derived growth factor receptor, beta polypeptide
Pdha1	Mm00468675_m1	Mm.34775	pyruvate dehydrogenase E1 alpha 1
Pik3c2g	Mm00440781_m1	Mm.333471	phosphatidylinositol 3-kinase, C2 domain containing, gamma polypeptide
Pik3cg	Mm00445038_m1	Mm.101369	phosphoinositide-3-kinase, catalytic, gamma polypeptide
Pik3r5	Mm00805206_m1	Mm.244960	phosphoinositide-3-kinase, regulatory subunit 5, p101
Pipox	Mm00477190_m1	Mm.8543	pipecolic acid oxidase
Pla2g4a	Mm00447040_m1	Mm.4186	phospholipase A2, group IVA (cytosolic, calcium-dependent)
Pla2g7	Mm00479105_m1	Mm.9277	phospholipase A2, group VII (platelet-activating factor acetylhydrolase, plasma)
Pla2r1	Mm00476896_m1	Mm.5092	phospholipase A2 receptor 1
Plau	Mm01274460_g1	Mm.4183	plasminogen activator, urokinase

For Peer Review Only

	Plcd4	Mm00455768_m1	Mm.290731	phospholipase C, delta 4
	Plce1	Mm00457691_m1	Mm.34031	phospholipase C, epsilon 1
	Pld4	Mm00626861_m1	Mm.203915	phospholipase D family, member 4
	Plekha2	Mm00504233_m1	Mm.261122	pleckstrin homology domain-containing, family A (phosphoinositide binding specific) member 2
	Pnmt	Mm00476993_m1	Mm.57030	phenylethanolamine-N-methyltransferase
	Por	Mm00435876_m1	Mm.3863	P450 (cytochrome) oxidoreductase
	Ppara	Mm00440939_m1	Mm.212789	peroxisome proliferator activated receptor alpha
	Ppm1l	Mm00618786_m1	Mm.40577	protein phosphatase 1 (formerly 2C)-like
	Prdx3	Mm00545848_m1	Mm.29821	peroxiredoxin 3
	Prdx5	Mm00465365_m1	Mm.279782	peroxiredoxin 5
	Prkcb	Mm00435749_m1	Mm.207496	protein kinase C, beta
	Prkcz	Mm00776345_g1	Mm.28561	protein kinase C, zeta
	Pros1	Mm01343426_m1	Mm.127156	protein S (alpha)
	Prtn3	Mm00478323_m1	Mm.2364	proteinase 3
	Psmb8	Mm01278979_m1	Mm.180191	proteasome (prosome, macropain) subunit, beta type 8 (large multifunctional peptidase 7)
	Psmb9	Mm00479004_m1	Mm.390983	proteasome (prosome, macropain) subunit, beta type 9 (large multifunctional peptidase 2)
	Ptgs2	Mm00478374_m1	Mm.292547	prostaglandin-endoperoxide synthase 2
	Ptpn22	Mm00501246_m1	Mm.395	protein tyrosine phosphatase, non-receptor type 22 (lymphoid)
	Ptpn6	Mm00469153_m1	Mm.271799	protein tyrosine phosphatase, non-receptor type 6
	Ptprc	Mm01293577_m1	Mm.391573	protein tyrosine phosphatase, receptor type, C
	Ptx3	Mm00477268_m1	Mm.276776	pentraxin related gene
	Pycard	Mm00445747_g1	Mm.24163	PYD and CARD domain containing
	Rac2	Mm00485472_m1	Mm.1972	RAS-related C3 botulinum substrate 2
	Rad23a	Mm00436249_g1	Mm.255539	RAD23a homolog (S. cerevisiae)
	Rdh14	Mm00502743_m1	Mm.119343	retinol dehydrogenase 14 (all-trans and 9-cis)
	Rela	Mm00501346_m1	Mm.249966	v-rel reticuloendotheliosis viral oncogene homolog A (avian)
	Relb	Mm00485664_m1	Mm.1741	avian reticuloendotheliosis viral (v-rel) oncogene related B
	Rnase1	Mm00726747_s1	Mm.235538	ribonuclease, RNase A family, 1 (pancreatic)
	Robo1	Mm00803879_m1	Mm.310772	roundabout homolog 1 (Drosophila)
	S100a8	Mm00496696_g1	Mm.21567	S100 calcium binding protein A8 (calgranulin A)
	Saa1	Mm00656927_g1	Mm.148800	serum amyloid A 1
	Sardh	Mm00454657_m1	Mm.278467	sarcosine dehydrogenase
	Scd1	Mm00772290_m1	Mm.267377	stearoyl-Coenzyme A desaturase 1
	Sdha	Mm01352366_m1	Mm.158231	succinate dehydrogenase complex, subunit A, flavoprotein (Fp)
	Serpina1a	Mm02748447_g1	Mm.439692	serine (or cysteine) peptidase inhibitor, clade A, member 1A
	Serpina1c; Serpina1a	Mm04207709_gH	Mm.439692	serine (or cysteine) peptidase inhibitor, clade A, member 1C
	Serpina1d	Mm00842094_mH	Mm.439695	serine (or cysteine) peptidase inhibitor, clade A, member 1D
	Serpina1d; Serpina1b	Mm04207706_gH	Mm.439692	serine (or cysteine) preptidase inhibitor, clade A, member 1B
	Serpina1e	Mm00833655_m1	Mm.312593	serine (or cysteine) peptidase inhibitor, clade A, member 1E
	Serpina6	Mm00432327_m1	Mm.290079	serine (or cysteine) peptidase inhibitor, clade A, member 6
	Serpine1	Mm00435860_m1	Mm.250422	serine (or cysteine) peptidase inhibitor, clade E, member 1
	Serping1	Mm00437834_m1	Mm.38888	serine (or cysteine) peptidase inhibitor, clade G, member 1
	Sh3bp2	Mm00449397_m1	Mm.5012	SH3-domain binding protein 2
	Sigirr	Mm01275624_g1	Mm.38017	single immunoglobulin and toll-interleukin 1 receptor (TIR) domain
	Slc2a4	Mm01245502_m1	Mm.10661	solute carrier family 2 (facilitated glucose transporter), member 4

For Peer Review Only

Socs3	Mm00545913_s1	Mm.3468	suppressor of cytokine signaling 3
Sod2	Mm01313000_m1	Mm.290876	superoxide dismutase 2, mitochondrial
Sod3	Mm01213380_s1	Mm.2407	superoxide dismutase 3, extracellular
Sord	Mm00455377_g1	Mm.371580	sorbitol dehydrogenase
Spi1	Mm00488142_m1	Mm.1302	spleen focus forming virus (SFFV) proviral integration oncogene
Spn	Mm01164549_m1	Mm.283714	sialophorin
Spp1	Mm00436767_m1	Mm.288474	secreted phosphoprotein 1
Srr	Mm01246014_m1	Mm.131443	serine racemase
Stat1	Mm00439531_m1	Mm.277406	signal transducer and activator of transcription 1
Stat3	Mm01219775_m1	Mm.249934	signal transducer and activator of transcription 3
Stat4	Mm00448890_m1	Mm.1550	signal transducer and activator of transcription 4
Suox	Mm00620388_g1	Mm.23352	sulfite oxidase
Surf1	Mm00489041_g1	Mm.347512	surfeit gene 1
Syk	Mm01333032_m1	Mm.375031	spleen tyrosine kinase
Tap1	Mm00443188_m1	Mm.482076	transporter 1, ATP-binding cassette, sub-family B (MDR/TAP)
Tap2	Mm01277033_m1	Mm.14814	transporter 2, ATP-binding cassette, sub-family B (MDR/TAP)
Tapbp	Mm00493417_m1	Mm.154457	TAP binding protein
Tgfb1	Mm01178820_m1	Mm.248380	transforming growth factor, beta 1
Tgfbr1	Mm00436964_m1	Mm.197552	transforming growth factor, beta receptor I
Thbs2	Mm01279240_m1	Mm.26688	thrombospondin 2
Timp3	Mm00441826_m1	Mm.4871	tissue inhibitor of metalloproteinase 3
Tlr1	Mm00446095_m1	Mm.273024	toll-like receptor 1
Tlr13	Mm01233819_m1	Mm.336203	toll-like receptor 13
Tlr2	Mm00442346_m1	Mm.87596	toll-like receptor 2
Tlr4	Mm00445273_m1	Mm.38049	toll-like receptor 4
Tlr7	Mm00446590_m1	Mm.23979	toll-like receptor 7
Tlr9	Mm00446193_m1	Mm.44889	toll-like receptor 9
Tmem173	Mm01158117_m1	Mm.45995	transmembrane protein 173
Tnf	Mm00443258_m1	Mm.1293	tumor necrosis factor
Tnfaip3	Mm00437121_m1	Mm.116683	tumor necrosis factor, alpha-induced protein 3
Tnfrsf12a	Mm01302476_g1	Mm.28518	tumor necrosis factor receptor superfamily, member 12a
Tnfrsf13b	Mm00840182_m1	Mm.265915	tumor necrosis factor receptor superfamily, member 13b
Tnfrsf13c	Mm00840578_g1	Mm.240047	tumor necrosis factor receptor superfamily, member 13c
Tnfrsf17	Mm00495683_m1	Mm.12935	tumor necrosis factor receptor superfamily, member 17
Tnfsf12	Mm02583406_s1	Mm.8983	tumor necrosis factor (ligand) superfamily, member 12
Tnfsf13	Mm03809849_s1	Mm.8983	tumor necrosis factor (ligand) superfamily, member 13
Tnfsf13b	Mm00446347_m1	Mm.28835	tumor necrosis factor (ligand) superfamily, member 13b
Tnfsf4	Mm00437214_m1	Mm.4994	tumor necrosis factor (ligand) superfamily, member 4
Tnip1	Mm01288484_m1	Mm.259671	TNFAIP3 interacting protein 1
Tnip2	Mm00460482_m1	Mm.28615	TNFAIP3 interacting protein 2
Tnip3	Mm01181626_m1	Mm.117558	TNFAIP3 interacting protein 3
Traf1	Mm00493827_m1	Mm.239514	TNF receptor-associated factor 1
Traf2	Mm00801978_m1	Mm.3399	TNF receptor-associated factor 2
Trak1	Mm00613053_m1	Mm.491112	trafficking protein, kinesin binding 1
Trem2	Mm04209424_g1	Mm.261623	triggering receptor expressed on myeloid cells 2
Tst	Mm01195231_m1	Mm.15312	thiosulfate sulfurtransferase, mitochondrial

For Peer Review Only

Txnrd2	Mm00496766_m1	Mm.390906	thioredoxin reductase 2
Tyrobp	Mm00449152_m1	Mm.46301	TYRO protein tyrosine kinase binding protein
Ugt2b34	Mm00655373_m1	Mm.281844	UDP glucuronosyltransferase 2 family, polypeptide B34
Ugt2b35	Mm00655596_m1	Mm.312095	UDP glucuronosyltransferase 2 family, polypeptide B35
Umod	Mm00447649_m1	Mm.10826	uromodulin
Uqcrc1	Mm00445911_m1	Mm.335460	ubiquinol-cytochrome c reductase core protein 1
Uqcrc2	Mm00445961_m1	Mm.334206	ubiquinol cytochrome c reductase core protein 2
Uqcrfs1	Mm00481849_m1	Mm.181933	ubiquinol-cytochrome c reductase, Rieske iron-sulfur polypeptide 1
Vamp3	Mm01268442_g1	Mm.273930	vesicle-associated membrane protein 3
Vav1	Mm01232047_m1	Mm.248172	vav 1 oncogene
Vcam1	Mm01320970_m1	Mm.440909	vascular cell adhesion molecule 1
Vegfa	Mm01281449_m1	Mm.282184	vascular endothelial growth factor A
Vegfc	Mm00437310_m1	Mm.1402	vascular endothelial growth factor C
Was	Mm00494167_m1	Mm.4735	Wiskott-Aldrich syndrome homolog (human)
Zbtb46	Mm00511327_m1	Mm.486504	zinc finger and BTB domain containing 46
Zfp36	Mm00457144_m1	Mm.389856	zinc finger protein 36

For Peer Review Only

Table S2.- List of genes induced by C4BP(β-) treatment (FC ≥ 1.8)

Gene Symbol	Log_2(FC) C4BP(β-)	Assay ID	UniGene ID	Gene name
Chga	9,2	Mm00514341_m1	Mm.4137	chromogranin A
Pnmt	9,1	Mm00476993_m1	Mm.57030	phenylethanolamine-N-methyltransferase
Adh7	4,1	Mm00507750_m1	Mm.8473	alcohol dehydrogenase 7 (class IV), mu or sigma polypeptide
Robo1	1,1	Mm00803879_m1	Mm.310772	roundabout homolog 1 (Drosophila)
Serpina1a	1,0	Mm02748447_g1	Mm.439692	serine (or cysteine) peptidase inhibitor, clade A, member 1A
Adh1	1,0	Mm00507711_m1	Mm.2409	alcohol dehydrogenase 1 (class I)
Serpina6	1,0	Mm00432327_m1	Mm.290079	serine (or cysteine) peptidase inhibitor, clade A, member 6
Igfbp6	0,9	Mm00599696_m1	Mm.358609	insulin-like growth factor binding protein 6
Ccr6	-0,9	Mm99999114_s1	Mm.8007	chemokine (C-C motif) receptor 6
Cst7	-0,9	Mm00438349_m1	Mm.12965	cystatin F (leukocystatin)
Psmb8	-0,9	Mm01278979_m1	Mm.180191	proteasome (prosome, macropain) subunit, beta type 8 (large multifunctional peptidase 7)
Cd22	-0,9	Mm00515432_m1	Mm.260994	CD22 antigen
Havcr1	-0,9	Mm00506686_m1	Mm.17771	hepatitis A virus cellular receptor 1
Blk	-0,9	Mm00432077_m1	Mm.3962	B lymphoid kinase
Cd3d	-0,9	Mm00442746_m1	Mm.4527	CD3 antigen, delta polypeptide
Lat	-1,0	Mm00456761_m1	Mm.10280	linker for activation of T cells
Tnfrsf13c	-1,1	Mm00840578_g1	Mm.240047	tumor necrosis factor receptor superfamily, member 13c
Irf7	-1,2	Mm00516793_g1	Mm.3233	interferon regulatory factor 7
Prtn3	-1,3	Mm00478323_m1	Mm.2364	proteinase 3
Ms4a1	-1,4	Mm00545909_m1	Mm.4046	membrane-spanning 4-domains, subfamily A, member 1
S100a8	-1,6	Mm00496696_g1	Mm.21567	S100 calcium binding protein A8 (calgranulin A)
Cd19	-1,6	Mm00515420_m1	Mm.4360	CD19 antigen
Il12a	-2,8	Mm00434165_m1	Mm.103783	interleukin 12a
Saa1	-3,4	Mm00656927_g1	Mm.148800	serum amyloid A 1

FC: Fold change

For Peer Review Only

Table S3.- List of genes induced by CYP treatment (FC ≥ 1.8)

Gene Symbol	Log_2(FC) CYP	Assay ID	UniGene ID	Gene name
Serpina6	2,5	Mm00432327_m1	Mm.290079	serine (or cysteine) peptidase inhibitor, clade A, member 6
Serpina1d	2,1	Mm00842094_mH	Mm.439695	serine (or cysteine) peptidase inhibitor, clade A, member 1D
Npy	1,7	Mm03048253_m1	Mm.154796	neuropeptide Y
Igfbp1	1,6	Mm00515154_m1	Mm.21300	insulin-like growth factor binding protein 1
C8a	1,5	Mm00521627_m1	Mm.197638	complement component 8, alpha polypeptide
Serpina1a	1,5	Mm02748447_g1	Mm.439692	serine (or cysteine) peptidase inhibitor, clade A, member 1A
Aldh6a1	1,3	Mm00506227_m1	Mm.247510	aldehyde dehydrogenase family 6, subfamily A1
Ndrg2	1,2	Mm00443481_g1	Mm.26722	N-myc downstream regulated gene 2
Ace	1,2	Mm00802048_m1	Mm.754	angiotensin I converting enzyme (peptidyl-dipeptidase A) 1
Bckdhb	1,1	Mm01177077_m1	Mm.12819	branched chain ketoacid dehydrogenase E1, beta polypeptide
Slc2a4	1,1	Mm01245502_m1	Mm.10661	solute carrier family 2 (facilitated glucose transporter), member 4
Aldh4a1	1,1	Mm00615268_m1	Mm.273571	aldehyde dehydrogenase 4 family, member A1
Plcd4	1,1	Mm00455768_m1	Mm.290731	phospholipase C, delta 4
Por	1,1	Mm00435876_m1	Mm.3863	P450 (cytochrome) oxidoreductase
Fmo1	1,1	Mm00515795_m1	Mm.976	flavin containing monooxygenase 1
Pik3c2g	1,1	Mm00440781_m1	Mm.333471	phosphatidylinositol 3-kinase, C2 domain containing, gamma polypeptide
Klkb1	1,0	Mm00434658_m1	Mm.482691	kallikrein B, plasma 1
Cbs	1,0	Mm00460654_m1	Mm.206417	cystathionine beta-synthase
Sod2	1,0	Mm01313000_m1	Mm.290876	superoxide dismutase 2, mitochondrial
Ugt2b34	1,0	Mm00655373_m1	Mm.281844	UDP glucuronosyltransferase 2 family, polypeptide B34
Fmo4	1,0	Mm00467393_m1	Mm.155164	flavin containing monooxygenase 4
Nox4	1,0	Mm00479246_m1	Mm.31748	NADPH oxidase 4
Ahcyl2	1,0	Mm00619649_m1	Mm.210899	S-adenosylhomocysteine hydrolase-like 2
Scd1	1,0	Mm00772290_m1	Mm.267377	stearoyl-Coenzyme A desaturase 1
Prkcz	1,0	Mm00776345_g1	Mm.28561	protein kinase C, zeta
Cat	1,0	Mm00437992_m1	Mm.4215	catalase
Adhfe1	1,0	Mm00613830_m1	Mm.28514	alcohol dehydrogenase, iron containing, 1
Serpina1d; Serpina1b	1,0	Mm04207706_gH	Mm.439692	serine (or cysteine) preptidase inhibitor, clade A, member 1B
Idh3b	0,9	Mm00504589_m1	Mm.29590	isocitrate dehydrogenase 3 (NAD+) beta
Sardh	0,9	Mm00454657_m1	Mm.278467	sarcosine dehydrogenase
Sord	0,9	Mm00455377_g1	Mm.371580	sorbitol dehydrogenase
Id1	0,9	Mm00775963_g1	Mm.444	inhibitor of DNA binding 1
Aldh9a1	0,9	Mm00480240_m1	Mm.292539	aldehyde dehydrogenase 9, subfamily A1
Sdha	0,9	Mm01352366_m1	Mm.158231	succinate dehydrogenase complex, subunit A, flavoprotein (Fp)
Bckdha	0,9	Mm00476112_m1	Mm.25848	branched chain ketoacid dehydrogenase E1, alpha polypeptide
Suox	0,9	Mm00620388_g1	Mm.23352	sulfite oxidase
Tst	0,9	Mm01195231_m1	Mm.15312	thiosulfate sulfurtransferase, mitochondrial
Pcca	0,9	Mm00454899_m1	Mm.23876	propionyl-Coenzyme A carboxylase, alpha polypeptide
Idh3g	0,9	Mm00599686_g1	Mm.14825	isocitrate dehydrogenase 3 (NAD+), gamma
Hnf4a	0,9	Mm01247712_m1	Mm.202383	hepatic nuclear factor 4, alpha
Ndufa10	0,9	Mm00600325_m1	Mm.248778	NADH dehydrogenase (ubiquinone) 1 alpha subcomplex 10
Ppm1l	0,9	Mm00618786_m1	Mm.40577	protein phosphatase 1 (formerly 2C)-like
Prdx3	0,9	Mm00545848_m1	Mm.29821	peroxiredoxin 3
Got1	0,9	Mm01195792_g1	Mm.19039	glutamic-oxaloacetic transaminase 1, soluble
Ndufaf1	0,9	Mm00452828_m1	Mm.5390	NADH dehydrogenase (ubiquinone) 1 alpha subcomplex, assembly factor 1
Gss	0,9	Mm00515065_m1	Mm.252316	glutathione synthetase
Auh	0,9	Mm00479363_m1	Mm.252034	AU RNA binding protein/enoyl-coenzyme A hydratase
Ndufs7	0,9	Mm01144210_m1	Mm.28712	NADH dehydrogenase (ubiquinone) Fe-S protein 7
Atp5f1	0,9	Mm01296543_g1	Mm.251152	ATP synthase, H+ transporting, mitochondrial F0 complex, subunit B1
Timp3	0,8	Mm00441826_m1	Mm.4871	tissue inhibitor of metalloproteinase 3
Aldh2	0,8	Mm00477463_m1	Mm.284446	aldehyde dehydrogenase 2, mitochondrial
Stat3	-0,9	Mm01219775_m1	Mm.249934	signal transducer and activator of transcription 3
Irf1	-0,9	Mm01288580_m1	Mm.105218	interferon regulatory factor 1
B2m	-0,9	Mm00437762_m1	Mm.163	beta-2 microglobulin
Cx3cl1	-0,9	Mm00436454_m1	Mm.103711	chemokine (C-X3-C motif) ligand 1

For Peer Review Only

Ctgf	-0,9	Mm01192932_g1	Mm.390287	connective tissue growth factor
Hmox1	-0,9	Mm00516005_m1	Mm.276389	heme oxygenase 1
F3	-0,9	Mm00438853_m1	Mm.273188	coagulation factor III
Tnfaip3	-0,9	Mm00437121_m1	Mm.116683	tumor necrosis factor, alpha-induced protein 3
Icam1	-0,9	Mm00516023_m1	Mm.435508	intercellular adhesion molecule 1
Tgfb1	-1,0	Mm01178820_m1	Mm.248380	transforming growth factor, beta 1
Sh3bp2	-1,0	Mm00449397_m1	Mm.5012	SH3-domain binding protein 2
Lyn	-1,0	Mm01217488_m1	Mm.317331	Yamaguchi sarcoma viral (v-yes-1) oncogene homolog
Traf1	-1,0	Mm00493827_m1	Mm.239514	TNF receptor-associated factor 1
Apoe	-1,0	Mm01307193_g1	Mm.305152	apolipoprotein E
Tnfsf4	-1,0	Mm00437214_m1	Mm.4994	tumor necrosis factor (ligand) superfamily, member 4
Cebpb	-1,0	Mm00843434_s1	Mm.439656	CCAAT/enhancer binding protein (C/EBP), beta
Irf9	-1,0	Mm00492679_m1	Mm.2032	interferon regulatory factor 9
Inpp5d	-1,0	Mm00494987_m1	Mm.15105	inositol polyphosphate-5-phosphatase D
Igfbp6	-1,0	Mm00599696_m1	Mm.358609	insulin-like growth factor binding protein 6
Cfh	-1,0	Mm01299248_m1	Mm.8655	complement component factor h
Arpc1b	-1,0	Mm00834862_m1	Mm.30010	actin related protein 2/3 complex, subunit 1B
C1qc	-1,0	Mm00776126_m1	Mm.439732	complement component 1, q subcomponent, C chain
C4bp	-1,0	Mm00432150_m1	Mm.306720	complement component 4 binding protein
Cxcr4	-1,0	Mm01996749_s1	Mm.1401	chemokine (C-X-C motif) receptor 4
C1ra	-1,1	Mm04206253_g1	Mm.333375	complement component 1, r subcomponent A
Fga	-1,1	Mm00802584_m1	Mm.88793	fibrinogen alpha chain
Csf1	-1,1	Mm00432686_m1	Mm.795	colony stimulating factor 1 (macrophage)
C1s1	-1,1	Mm00663210_mH	Mm.219527	complement component 1, s subcomponent 1
Ikbke	-1,1	Mm00444862_m1	Mm.386783	inhibitor of kappaB kinase epsilon
Map3k8	-1,2	Mm00432637_m1	Mm.3275	mitogen-activated protein kinase kinase kinase 8
Pycard	-1,2	Mm00445747_g1	Mm.24163	PYD and CARD domain containing
Tlr4	-1,2	Mm00445273_m1	Mm.38049	toll-like receptor 4
Ccr1	-1,2	Mm00438260_s1	Mm.274927	chemokine (C-C motif) receptor 1
Cxcl9	-1,2	Mm00434946_m1	Mm.766	chemokine (C-X-C motif) ligand 9
Thbs2	-1,2	Mm01279240_m1	Mm.26688	thrombospondin 2
Psmb9	-1,2	Mm00479004_m1	Mm.390983	proteasome (prosome, macropain) subunit, beta type 9 (large multifunctional peptidase 2)
Il2rg	-1,3	Mm00442885_m1	Mm.2923	interleukin 2 receptor, gamma chain
Ncf1	-1,3	Mm00447921_m1	Mm.425296	neutrophil cytosolic factor 1
Relb	-1,3	Mm00485664_m1	Mm.1741	avian reticuloendotheliosis viral (v-rel) oncogene related B
Cxcl10	-1,3	Mm00445235_m1	Mm.877	chemokine (C-X-C motif) ligand 10
Mpo	-1,3	Mm01298424_m1	Mm.4668	myeloperoxidase
Fgg	-1,3	Mm00513575_m1	Mm.16422	fibrinogen gamma chain
Cd1d1	-1,4	Mm00783541_s1	Mm.1894	CD1d1 antigen
Ifng	-1,4	Mm01168134_m1	Mm.240327	interferon gamma
Fgb	-1,4	Mm00805336_m1	Mm.30063	fibrinogen beta chain
S100a8	-1,4	Mm00496696_g1	Mm.21567	S100 calcium binding protein A8 (calgranulin A)
Serping1	-1,4	Mm00437834_m1	Mm.38888	serine (or cysteine) peptidase inhibitor, clade G, member 1
Nfkbie	-1,4	Mm01269649_m1	Mm.57043	nuclear factor of kappa light polypeptide gene enhancer in B cells inhibitor, epsilon
Tlr7	-1,4	Mm00446590_m1	Mm.23979	toll-like receptor 7
Ptpn22	-1,4	Mm00501246_m1	Mm.395	protein tyrosine phosphatase, non-receptor type 22 (lymphoid)
Tlr1	-1,4	Mm00446095_m1	Mm.273024	toll-like receptor 1
Il33	-1,4	Mm00505403_m1	Mm.182359	interleukin 33
Nlrp3	-1,4	Mm00840904_m1	Mm.54174	NLR family, pyrin domain containing 3
Tnf	-1,4	Mm00443258_m1	Mm.1293	tumor necrosis factor
Mmp9	-1,5	Mm00442991_m1	Mm.4406	matrix metallopeptidase 9
Tap1	-1,5	Mm00443188_m1	Mm.482076	transporter 1, ATP-binding cassette, sub-family B (MDR/TAP)
Tnip3	-1,5	Mm01181626_m1	Mm.117558	TNFAIP3 interacting protein 3
Casp1	-1,5	Mm00438023_m1	Mm.1051	caspase 1
Prkcb	-1,5	Mm00435749_m1	Mm.207496	protein kinase C, beta
Il12b	-1,5	Mm00434174_m1	Mm.239707	interleukin 12b
Il27	-1,5	Mm00461162_m1	Mm.222632	interleukin 27
Ccl5	-1,5	Mm01302427_m1	Mm.284248	chemokine (C-C motif) ligand 5
Spi1	-1,5	Mm00488142_m1	Mm.1302	spleen focus forming virus (SFFV) proviral integration oncogene
Chga	-1,5	Mm00514341_m1	Mm.4137	chromogranin A

For Peer Review Only

Csf2rb	-1,5	Mm00655745_m1	Mm.235324	colony stimulating factor 2 receptor, beta, low-affinity (granulocyte-macrophage)
Tyrobp	-1,5	Mm00449152_m1	Mm.46301	TYRO protein tyrosine kinase binding protein
Itga4	-1,5	Mm01277951_m1	Mm.31903	integrin alpha 4
Il27ra	-1,6	Mm00497259_m1	Mm.38386	interleukin 27 receptor, alpha
Cst7	-1,6	Mm00438349_m1	Mm.12965	cystatin F (leukocystatin)
Spn	-1,6	Mm01164549_m1	Mm.283714	sialophorin
Ikzf1	-1,6	Mm01187882_m1	Mm.103545	IKAROS family zinc finger 1
Pik3cg	-1,6	Mm00445038_m1	Mm.101369	phosphoinositide-3-kinase, catalytic, gamma polypeptide
Lck	-1,6	Mm00802897_m1	Mm.293753	lymphocyte protein tyrosine kinase
Stat4	-1,6	Mm00448890_m1	Mm.1550	signal transducer and activator of transcription 4
Tlr9	-1,6	Mm00446193_m1	Mm.44889	toll-like receptor 9
Tnfsf13b	-1,6	Mm00446347_m1	Mm.28835	tumor necrosis factor (ligand) superfamily, member 13b
Psmb8	-1,6	Mm01278979_m1	Mm.180191	proteasome (prosome, macropain) subunit, beta type 8 (large multifunctional peptidase 7)
Trem2	-1,6	Mm04209424_g1	Mm.261623	triggering receptor expressed on myeloid cells 2
Cx3cr1	-1,6	Mm02620111_s1	Mm.44065	chemokine (C-X3-C motif) receptor 1
Was	-1,6	Mm00494167_m1	Mm.4735	Wiskott-Aldrich syndrome homolog (human)
Il27ra	-1,6	Mm00497259_m1	Mm.38386	interleukin 27 receptor, alpha
Rac2	-1,6	Mm00485472_m1	Mm.1972	RAS-related C3 botulinum substrate 2
Cd83	-1,6	Mm00486868_m1	Mm.57175	CD83 antigen
Vav1	-1,6	Mm01232047_m1	Mm.248172	vav 1 oncogene
Btk	-1,7	Mm00442712_m1	Mm.4475	Bruton agammaglobulinemia tyrosine kinase
Blk	-1,7	Mm00432077_m1	Mm.3962	B lymphoid kinase
Ccr7	-1,7	Mm01301785_m1	Mm.2932	chemokine (C-C motif) receptor 7
Pdcd1lg2	-1,7	Mm00451734_m1	Mm.116737	programmed cell death 1 ligand 2
Cd22	-1,7	Mm00515432_m1	Mm.260994	CD22 antigen
Tmem173	-1,7	Mm01158117_m1	Mm.45995	transmembrane protein 173
Cd86	-1,7	Mm00444543_m1	Mm.1452	CD86 antigen
Itgb2	-1,7	Mm00434513_m1	Mm.1137	integrin beta 2
Hck	-1,7	Mm01241463_m1	Mm.715	hemopoietic cell kinase
Tnfrsf12a	-1,7	Mm01302476_g1	Mm.28518	tumor necrosis factor receptor superfamily, member 12a
Clec7a	-1,7	Mm01183349_m1	Mm.239516	C-type lectin domain family 7, member a
Cd79b	-1,7	Mm00434143_m1	Mm.2987	CD79B antigen
Icos	-1,7	Mm00497600_m1	Mm.42044	inducible T cell co-stimulator
Tlr13	-1,8	Mm01233819_m1	Mm.336203	toll-like receptor 13
Fasl	-1,8	Mm00438864_m1	Mm.3355	Fas ligand (TNF superfamily, member 6)
Fcer1g	-1,8	Mm02343757_m1	Mm.22673	Fc receptor, IgE, high affinity I, gamma polypeptide
Aim2	-1,8	Mm01295719_m1	Mm.131453	absent in melanoma 2
Pld4	-1,8	Mm00626861_m1	Mm.203915	phospholipase D family, member 4
C1qa	-1,8	Mm00432142_m1	Mm.439957	complement component 1, q subcomponent, alpha polypeptide
Cd276	-1,8	Mm00506020_m1	Mm.5356	CD276 antigen
Tnfrsf13b	-1,8	Mm00840182_m1	Mm.265915	tumor necrosis factor receptor superfamily, member 13b
Osmr	-1,8	Mm01307326_m1	Mm.10760	oncostatin M receptor
Cd74	-1,8	Mm00658576_m1	Mm.439737	CD74 antigen (invariant polypeptide of major histocompatibility complex, class II antigen-associated)
Prtn3	-1,8	Mm00478323_m1	Mm.2364	proteinase 3
Syk	-1,8	Mm01333032_m1	Mm.375031	spleen tyrosine kinase
Cd48	-1,9	Mm00455932_m1	Mm.1738	CD48 antigen
Il10ra	-1,9	Mm00434151_m1	Mm.379327	interleukin 10 receptor, alpha
Cxcl1	-1,9	Mm04207460_m1	Mm.21013	chemokine (C-X-C motif) ligand 1
Irf7	-1,9	Mm00516793_g1	Mm.3233	interferon regulatory factor 7
Clec10a	-1,9	Mm00546125_g1	Mm.252405	C-type lectin domain family 10, member A
C3ar1	-1,9	Mm02620006_s1	Mm.2408	complement component 3a receptor 1
C1qb	-1,9	Mm01179619_m1	Mm.2570	complement component 1, q subcomponent, beta polypeptide
Fcgr3	-1,9	Mm00438882_m1	Mm.22119	Fc receptor, IgG, low affinity III
Cd3g	-1,9	Mm00438095_m1	Mm.335106	CD3 antigen, gamma polypeptide
Clu	-1,9	Mm01197002_m1	Mm.200608	clusterin
Ltb	-2,0	Mm00434774_g1	Mm.1715	lymphotoxin B
Lcp2	-2,0	Mm01187570_m1	Mm.265350	lymphocyte cytosolic protein 2
Ifi202b	-2,0	Mm00839397_m1	Mm.218770	interferon activated gene 202B
Lat	-2,0	Mm00456761_m1	Mm.10280	linker for activation of T cells
Vcam1	-2,0	Mm01320970_m1	Mm.440909	vascular cell adhesion molecule 1

For Peer Review Only

Il1r2	-2,0	Mm00439629_m1	Mm.1349	interleukin 1 receptor, type II
Pik3r5	-2,0	Mm00805206_m1	Mm.244960	phosphoinositide-3-kinase, regulatory subunit 5, p101
Ptprc	-2,0	Mm01293577_m1	Mm.391573	protein tyrosine phosphatase, receptor type, C
Spp1	-2,0	Mm00436767_m1	Mm.288474	secreted phosphoprotein 1
Ccr2	-2,0	Mm00438270_m1	Mm.6272	chemokine (C-C motif) receptor 2
Col1a2	-2,1	Mm00483888_m1	Mm.277792	collagen, type I, alpha 2
Fn1	-2,1	Mm01256744_m1	Mm.193099	fibronectin 1
Cd80	-2,1	Mm00711660_m1	Mm.89474	CD80 antigen
Foxp3	-2,1	Mm00475162_m1	Mm.182291	forkhead box P3
Cd40lg	-2,1	Mm00441911_m1	Mm.4861	CD40 ligand
Clec4n	-2,2	Mm00490934_m1	Mm.271782	C-type lectin domain family 4, member n
Pnmt	-2,2	Mm00476993_m1	Mm.57030	phenylethanolamine-N-methyltransferase
Ctla4	-2,2	Mm00486849_m1	Mm.390	cytotoxic T-lymphocyte-associated protein 4
Msr1	-2,2	Mm00446214_m1	Mm.239291	macrophage scavenger receptor 1
Il1b	-2,2	Mm00434228_m1	Mm.222830	interleukin 1 beta
Cd28	-2,2	Mm00483137_m1	Mm.255003	CD28 antigen
Ccr6	-2,2	Mm99999114_s1	Mm.8007	chemokine (C-C motif) receptor 6
Cd3d	-2,3	Mm00442746_m1	Mm.4527	CD3 antigen, delta polypeptide
Il10	-2,3	Mm00439614_m1	Mm.874	interleukin 10
Gpnmb	-2,3	Mm01328587_m1	Mm.302602	glycoprotein (transmembrane) nmb
Serpine1	-2,3	Mm00435860_m1	Mm.250422	serine (or cysteine) peptidase inhibitor, clade E, member 1
Ctss	-2,3	Mm01255859_m1	Mm.3619	cathepsin S
Ccl9	-2,3	Mm00441260_m1	Mm.416125	chemokine (C-C motif) ligand 9
Cd19	-2,3	Mm00515420_m1	Mm.4360	CD19 antigen
Cd300lb	-2,3	Mm01701741_m1	Mm.185355	CD300 antigen like family member B
Fcgr4	-2,3	Mm00519988_m1	Mm.251254	Fc receptor, IgG, low affinity IV
Cd5	-2,4	Mm00432417_m1	Mm.779	CD5 antigen
Tnfrsf17	-2,4	Mm00495683_m1	Mm.12935	tumor necrosis factor receptor superfamily, member 17
Tnfrsf13c	-2,4	Mm00840578_g1	Mm.240047	tumor necrosis factor receptor superfamily, member 13c
Irf4	-2,4	Mm00516431_m1	Mm.4677	interferon regulatory factor 4
Fcgr1	-2,4	Mm00438874_m1	Mm.150	Fc receptor, IgG, high affinity I
Ccl2	-2,4	Mm00441242_m1	Mm.290320	chemokine (C-C motif) ligand 2
Ms4a1	-2,5	Mm00545909_m1	Mm.4046	membrane-spanning 4-domains, subfamily A, member 1
Havcr1	-2,5	Mm00506686_m1	Mm.17771	hepatitis A virus cellular receptor 1
Cd14	-2,5	Mm00438094_g1	Mm.3460	CD14 antigen
Itgam	-2,5	Mm00434455_m1	Mm.262106	integrin alpha M
Il7r	-2,6	Mm00434295_m1	Mm.389	interleukin 7 receptor
C3	-2,7	Mm00437838_m1	Mm.19131	complement component 3
Cxcl2	-2,7	Mm00436450_m1	Mm.4979	chemokine (C-X-C motif) ligand 2
Ereg	-2,7	Mm00514794_m1	Mm.4791	epiregulin
Il17a	-2,7	Mm00439618_m1	Mm.5419	interleukin 17A
Col3a1	-2,7	Mm01254476_m1	Mm.249555	collagen, type III, alpha 1
Ccr5	-2,7	Mm01963251_s1	Mm.14302	chemokine (C-C motif) receptor 5
Socs3	-2,8	Mm00545913_s1	Mm.3468	suppressor of cytokine signaling 3
C6	-2,8	Mm00489521_m1	Mm.20247	complement component 6
Col1a1	-3,0	Mm00801666_g1	Mm.277735	collagen, type I, alpha 1
Cxcl13	-3,1	Mm04214185_s1	Mm.10116	chemokine (C-X-C motif) ligand 13
Saa1	-4,5	Mm00656927_g1	Mm.148800	serum amyloid A 1
Il1f6	-6,0	Mm00457645_m1	Mm.133095	interleukin 1 family, member 6

FC: Fold change

For Peer Review Only

Luque et al. (September 2019) KI-12-18-1865

Table S4.- Relevant enriched biological functions (IPA®) associated with differentially expressed renal genes from C4BP(β^-)-treated NZBW F1 mice.

Bio-function	# genes in dataset	Overlap p-value	Activation z-score*
Quantity of leukocytes	14	$2,91x10^{-11}$	**-2,836**
Activation of leukocytes	10	$6,03x10^{-10}$	-1,455
Quantity of mononuclear leukocytes	12	$6,06x10^{-10}$	**-2,541**
Quantity of lymphocytes	11	$6,87x10^{-9}$	**-2,839**
Leukocyte migration	9	$8,12x10^{-7}$	-1,966
Activation of lymphocytes	6	$5,71x10^{-6}$	-1,368
Quantity of B lymphocytes	6	$1,41x10^{-5}$	**-2,223**
Cell viability of lymphocytes	4	$4,15x10^{-5}$	-1,969
Cell movement of phagocytes	5	$3,53x10^{-4}$	**-2,211**
Cell movement of myeloid cells	5	$3,59x10^{-4}$	**-2,195**
Cellular infiltration by leukocytes	4	$1,90x10^{-3}$	-1,972
Inflammation of organ	5	$7,56x10^{-3}$	0,753

*Activation z-score is calculated by the IPA software and predicts whether a specific disease or bio-function is increased (positive z-score) or decreased (negative z-score) based on the experimental dataset. In bold are significant Bio-functions with z-score >2 or < -2.

For Peer Review Only

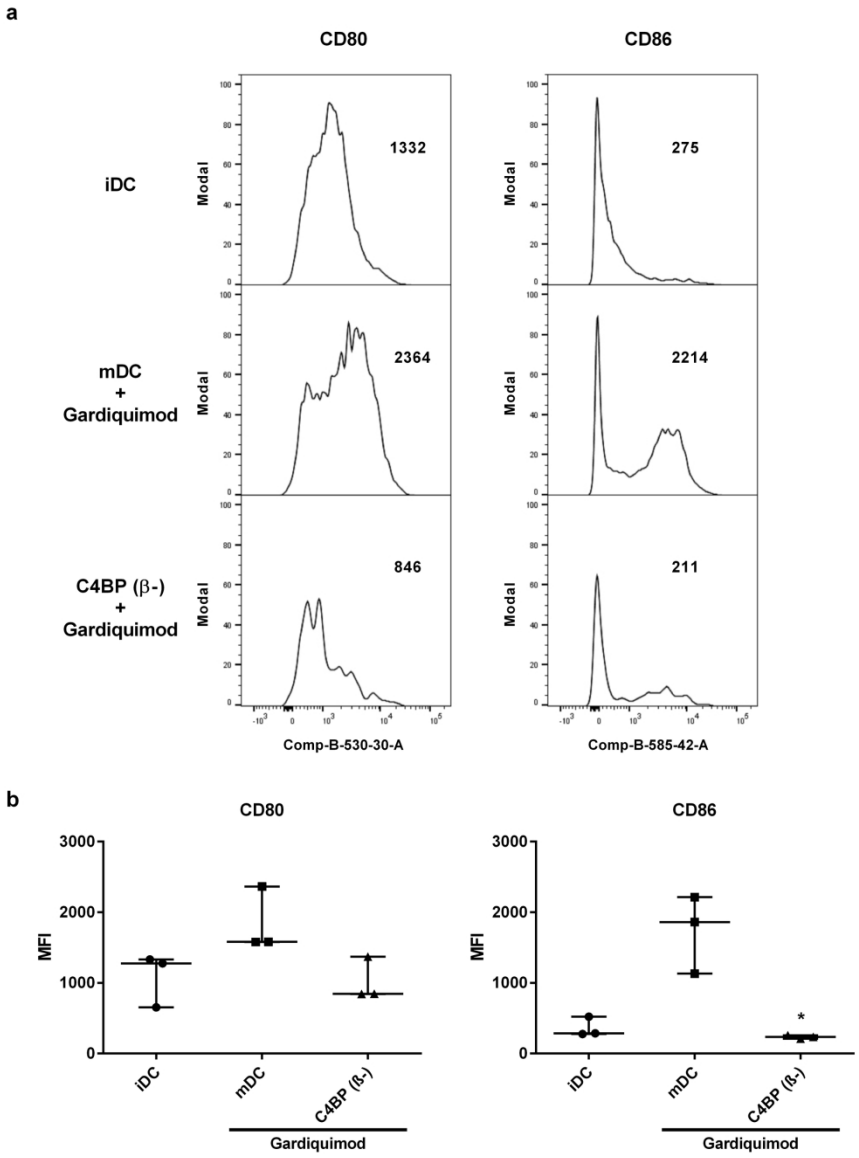

189x255mm (300 x 300 DPI)

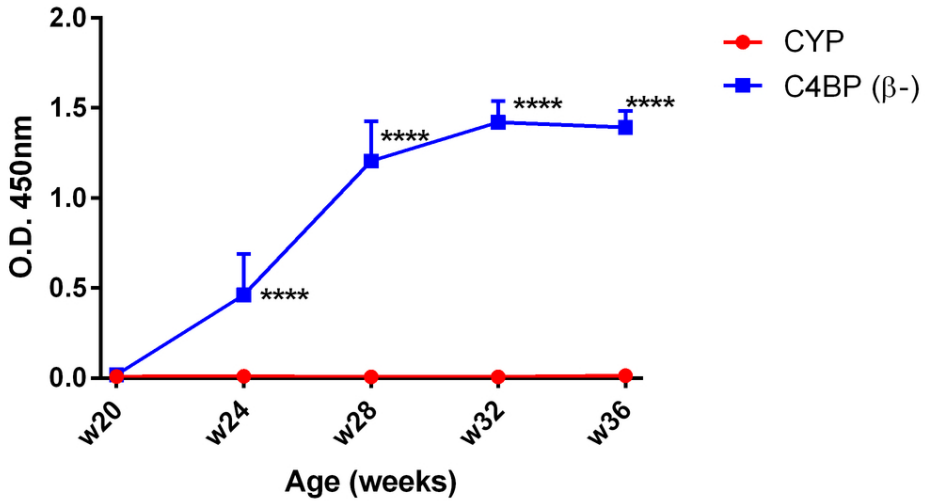

90x53mm (300 x 300 DPI)

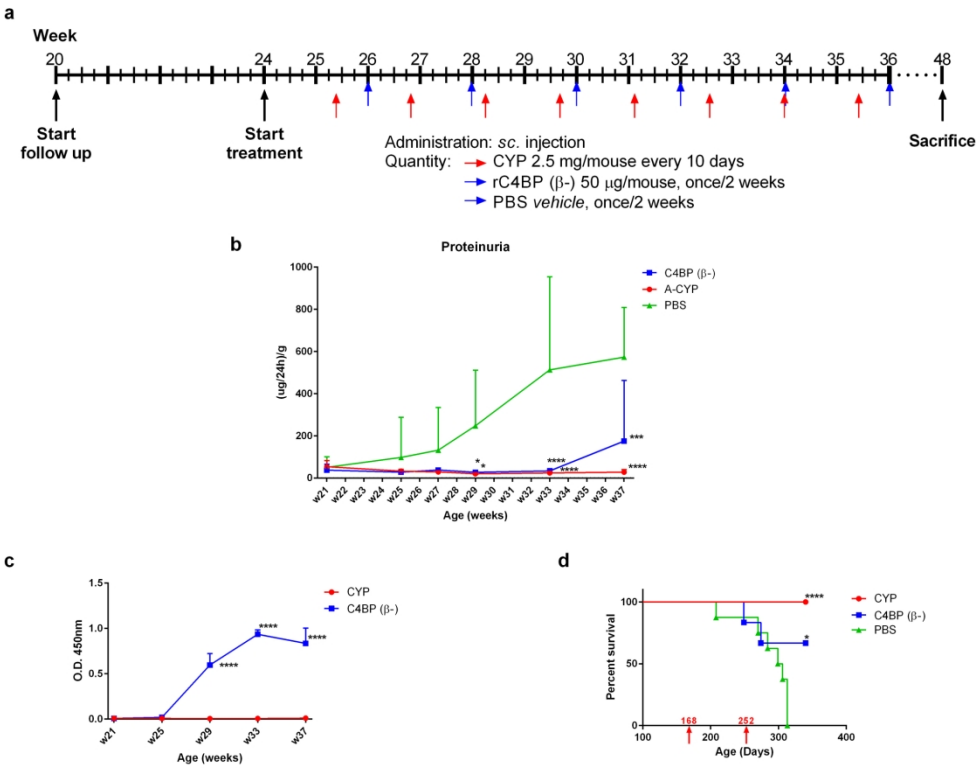

189x151mm (300 x 300 DPI)

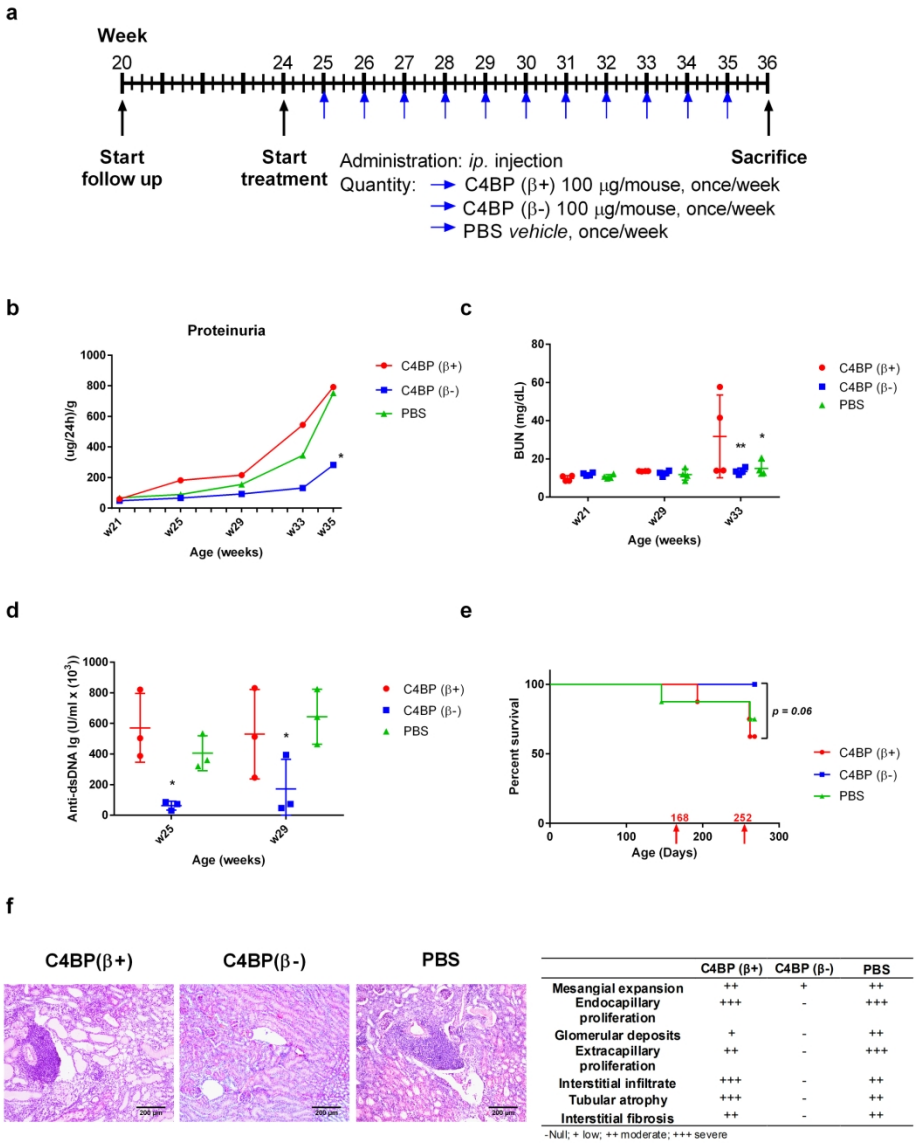

	C4BP (β+)	C4BP (β-)	PBS
Mesangial expansion	++	+	++
Endocapillary proliferation	+++	-	+++
Glomerular deposits	+	-	++
Extracapillary proliferation	++	-	+++
Interstitial infiltrate	+++	-	++
Tubular atrophy	+++	-	++
Interstitial fibrosis	++	-	++

-Null; + low; ++ moderate; +++ severe

189x240mm (300 x 300 DPI)

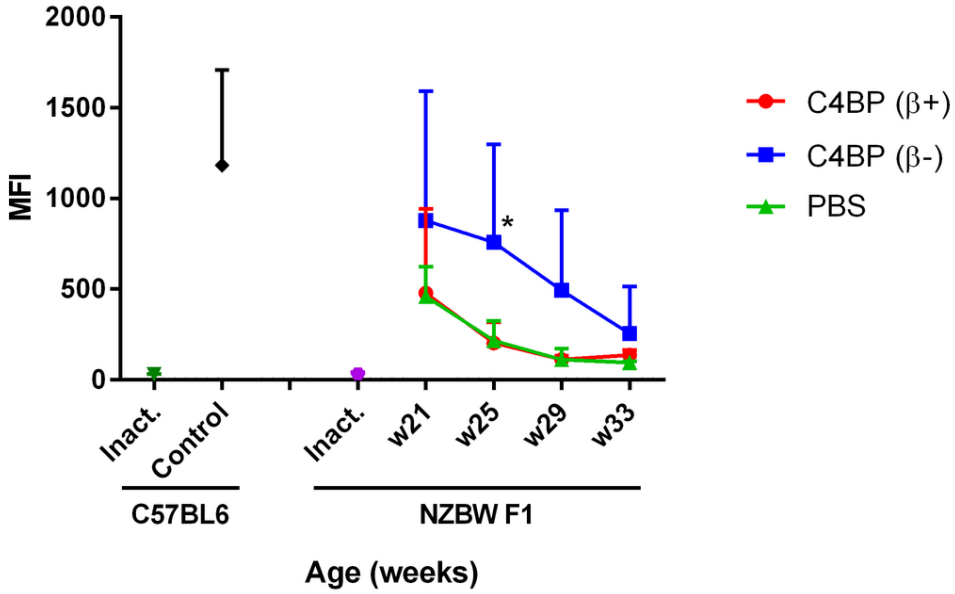

89x58mm (300 x 300 DPI)

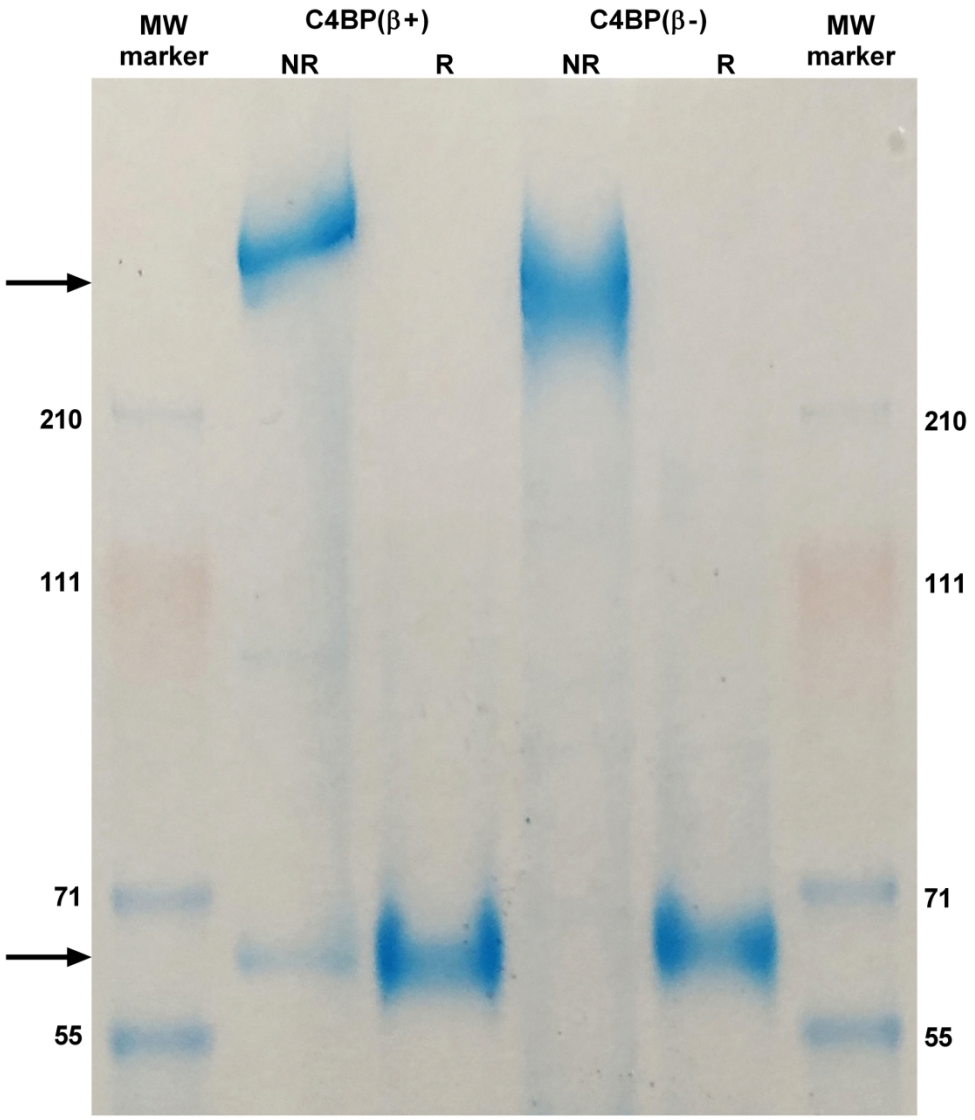

189x219mm (300 x 300 DPI)